JOURNAL OF GEOPHYSICAL RESEARCH, VOL. 108, NO. B6, 2287, doi:10.1029/2002JB001749, 2003

Distribution of interseismic slip rates and the potential for significant earthquakes on the Calaveras fault, central California

David M. Manaker
Department of Geology, University of California, Davis, California, USA

Roland Bürgmann
Department of Earth and Planetary Science, University of California, Berkeley, California, USA

William H. Prescott[1] and John Langbein
U. S. Geological Survey, Menlo Park, California, USA

Received 4 January 2002; revised 24 June 2002; accepted 10 January 2003; published 6 June 2003.

[1] The Calaveras fault is a major component of the San Andreas fault system in the San Francisco Bay area, that generated 13 earthquakes of $M_L > 5$ since 1850. In most recent $M_L > 5$ events, premain shock and postmain shock microseismicity is sparse in the region of coseismic slip. These aseismic areas are believed to represent locked patches of the fault that are accumulating strain to be released in $M_L > 5$ events. We analyze geodetic data to better characterize the spatial distribution of interseismic slip rates on the Calaveras fault, modeling the slip distribution in the seismogenic zone by inversion of over 25 years of surface deformation data. We use a regional fault model with the seismogenic zone of the Calaveras fault discretized into ~6 km × 3 km elements, employing a weighted least squares approach with smoothing and positivity constraints. Our discretized fault slip model consistently identifies regions of slip deficit in the seismogenic zone of the Calaveras fault that generally correspond to regions of decreased microseismicity and ruptures of previous moderate earthquakes. In particular, we find correspondence with the 1979 Coyote Lake and 1984 Morgan Hill events, as well as regions where historical earthquakes on the Coyote and the Sunol-San Ramon segments have occurred. Moment magnitude calculations based on the estimated slip deficit, fault area, and recurrence intervals agree with measured magnitudes of modern events and interpreted historical magnitudes. The results suggest that a combination of geodetically derived fault slip models and microseismicity distribution can be used to characterize seismic hazard. *INDEX TERMS:* 1206 Geodesy and Gravity: Crustal movements—interplate (8155); 1243 Geodesy and Gravity: Space geodetic surveys; 7223 Seismology: Seismic hazard assessment and prediction; *KEYWORDS:* Calaveras fault, fault models, earthquakes, California

Citation: Manaker, D. M., R. Bürgmann, W. H. Prescott, and J. Langbein, Distribution of interseismic slip rates and the potential for significant earthquakes on the Calaveras fault, central California, *J. Geophys. Res.*, *108*(B6), 2287, doi:10.1029/2002JB001749, 2003.

1. Introduction

[2] The Calaveras fault is a major part of the San Andreas fault system that forms the Pacific-North American plate boundary in northern California (Figure 1). It lies near major urban areas in the San Francisco Bay region (SFBR), including San Jose, Fremont, and the cities of the San Ramon Valley corridor and has the potential to cause significant loss of life and property. Since 1850, there have been 13 earthquakes of M_L 5 or greater on or near the Calaveras fault [*Oppenheimer et al.*, 1990], clearly suggesting that the fault presents a seismic hazard. However, the fault displays active creep along much of the surface trace, indicating that the situation at depth is more complicated than a single locked region. *Oppenheimer et al.* [1990] and *Oppenheimer and Lindh* [1992] analyzed the distribution of microseismicity and noted that in regions where $M_L > 5$ earthquakes occur, little seismicity above M_L 1.4 is exhibited and that premain shock and postmain shock microseismicity patterns are similar. In particular, they identified seven of these areas on the fault that correspond to the locations of historical events and interpret these areas to be locked and accumulating interseismic strain. Recently, precise relocations of 30 years of microseismicity on the Morgan Hill segment of the Calaveras fault by *Schaff et al.* [2002] show numerous repeating earthquake sequences and well-defined linear clusters and large voids. These large voids are on the scale of kilometers and are even better defined than the catalog hypocenters used by *Oppenheimer*

[1]Now at UNAVCO, Inc., Boulder, Colorado, USA.

0148-0227/03/2002JB001749$09.00

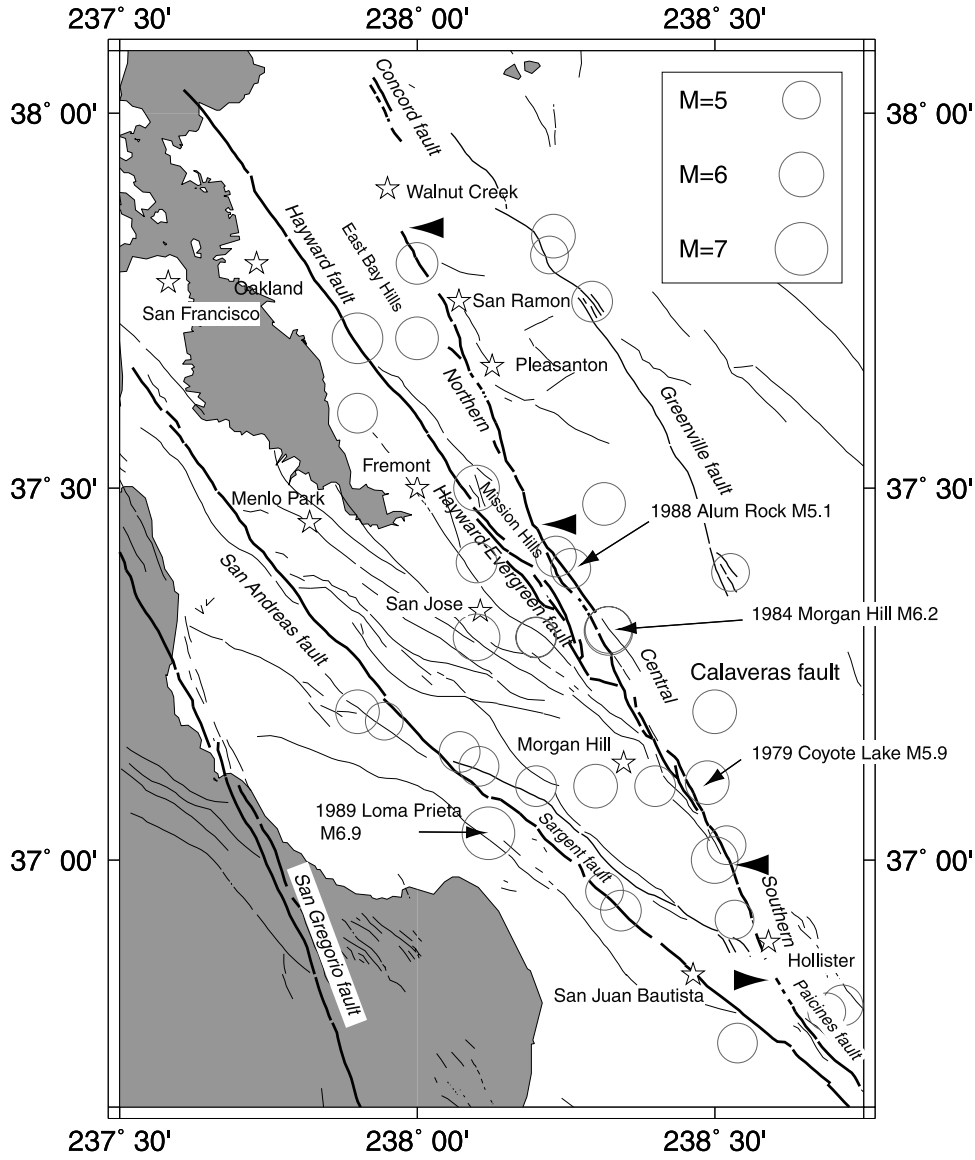

Figure 1. Regional map of the San Francisco Bay region. Major faults are shown by heavy black lines [*Jennings*, 1994]. Scaled circles show historical seismicity of $M_L \geq 5$ (*Oppenheimer et al.* [1990] and Northern California Seismic Network) from 1858 to 1998. Solid triangles define the southern, central, and northern segments of the Calaveras fault as used in this study. Also indicated are the locations of the recent series of three north propagating earthquakes [*Du and Aydin*, 1993].

et al. [1990] and *Oppenheimer and Lindh* [1992]. If these voids represent locked areas, then the interseismic slip rate distribution should show a deficit in these regions. We attempt to resolve the slip distribution at depth, using 25 years of surface deformation data to model the interseismic slip distribution on the Calaveras fault. Our results show a general correspondence between the aseismic areas and regions with modeled slip deficit, although the coarse nature of our model geometry does not provide for fine resolution of the aseismic regions. We also find agreement between the magnitudes of historical earthquakes and the seismic moment derived from the area, amount of slip deficit, and characteristic repeat times.

[3] The Calaveras fault has been the host of numerous events of moderate magnitude. Most notable is a recent northward propagating series of three earthquakes along the central segment (M_L 5.9 on 6 August 1979{Coyote Lake}, M_L 6.2 on 24 April 1984 {Morgan Hill}, and M_L 5.1 on 13 June 1988 {Alum Rock}) [*Du and Aydin*, 1993]. Also notable is an estimated M6.4 earthquake that occurred on the northern Calaveras fault on 3 July 1861 [*Rodgers and Halliday*, 1992; *Simpson et al.*, 1992]. Additionally, recent earthquake swarms in 1970 and 1990 with maximum magnitudes in the M4.0–4.5 range occurred near the northern end of the Calaveras fault [*Simpson et al.*, 1992; *Smith*, 1992]. Paleoseismic evidence suggests events with $M_w > 6.5$ are possible: At San Ysidro Creek near the southern end of the central Calaveras fault, evidence suggests earthquakes of $M_w \sim 7$, with at least 3 events producing surface rupture within the last 2000–4000 years [*Kelson et al.*, 1998]. There

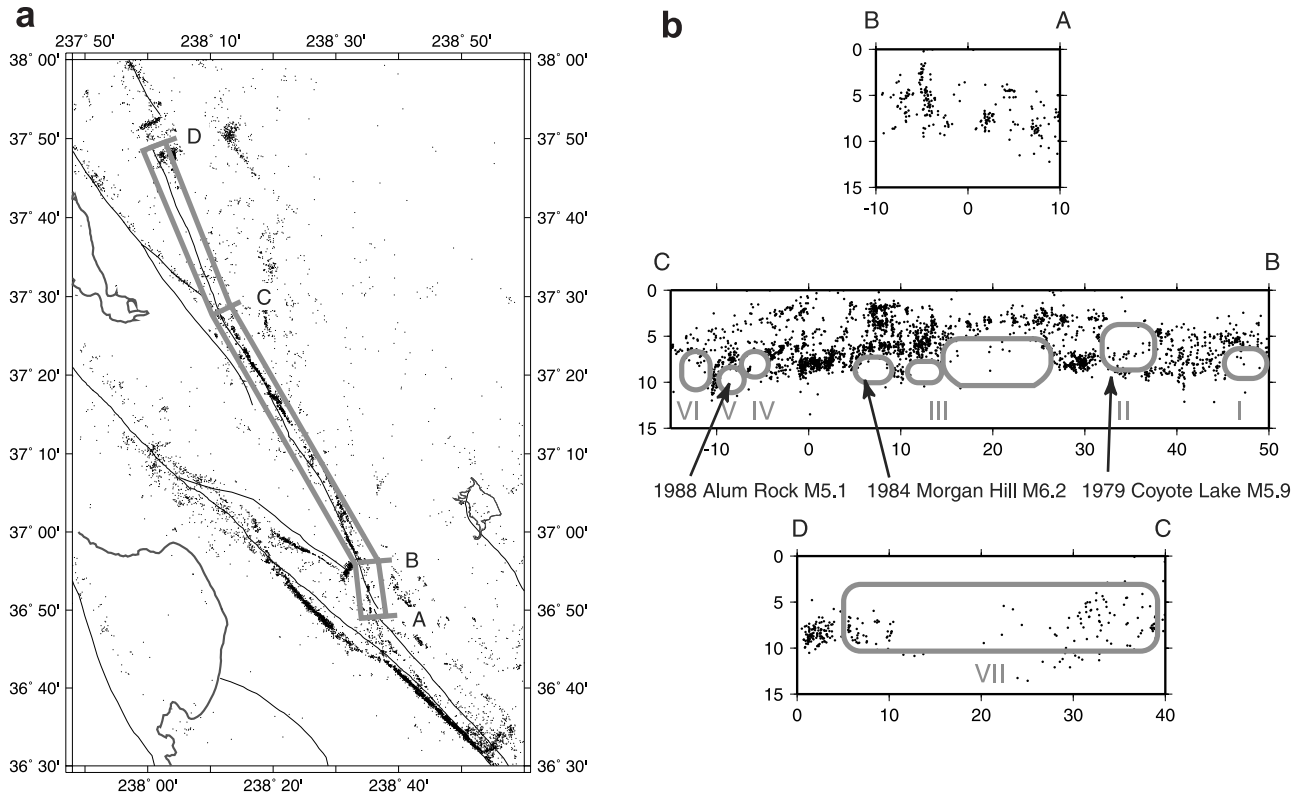

Figure 2. (a) Seismicity $M \geq 1.5$ from 1970 to 1998 for the southern San Francisco Bay region. All event locations from the Northern California Seismic Network catalog. Segments for seismicity cross sections indicated by the gray box with letters indicating profile endpoints used in Figure 2b. (b) Cross sections of seismicity ($M \geq 1.5$). Profile A–B shows seismicity for the period 1970–1998 (18 years). Profile B–C shows seismicity for the period 1990–1999 (8.5 years). Profile C–D shows seismicity for the period 1970–1998 (18 years). Note the greater level of seismicity for profile B–C. Suspected locked patches of the Calaveras fault from *Oppenheimer et al.* [1990] and *Oppenheimer and Lindh* [1992] are indicated by Roman numerals.

is also evidence for 5 to 6 events in the last 2500 years producing surface rupture on the northern Calaveras fault [*Kelson et al.*, 1996].

[4] The Calaveras fault is a ~140-km-long complex fault zone that exhibits a wide range of behavior along its trace (Figure 1). The fault connects with the Paicines fault, which trends subparallel (~N42°W) to the creeping San Andreas fault. South of Hollister, a complex triple junction region exists where the Calaveras fault takes a more northerly strike (~N19°W) and diverges from the Paicines and San Andreas faults. The southern Calaveras fault is well located, exhibiting surface creep along its trace and passing through the town of Hollister, where impressive deformation of man-made structures reflects rapid creep rates. Microseismicity is present on this segment, but at rates less that the central Calaveras fault (Figure 2). The transition from the southern to the central Calaveras fault is marked by another change in strike to ~N32°W north of Hollister at San Felipe Lake. This central segment is the host for most of the microseismicity and occasional moderate (M_L = 5–6.5) earthquakes that apparently repeat every 40–80 years [*Oppenheimer et al.*, 1990]. The central part of the fault lies within the rugged and largely unpopulated hills and ranchlands of the Diablo Range, which contributes to the lack of surface observations and geodetic data. Evidence for shallow slip and surface creep on the central segment is limited. Small aperture networks suggest shallow slip rates of 3 to 7 mm/yr at the northern end [*Prescott et al.*, 1981] and alignment arrays suggest shallow slip rates of 13 to 18 mm/yr at the southern end (J. Galehouse, personal communication, 1999). The central segment extends northward to the Calaveras reservoir, where a change in strike to ~N25°W marks the transition to the northern segment. The northern segment is largely aseismic; however, the 1861 event and the above mentioned paleoseismic evidence suggests a potential for damaging earthquakes.

[5] The northern part of the central segment and northern segment trend subparallel to the Evergreen-Hayward fault system for a distance of ~50 km. The region of overlap is characterized by uplift, folding and reverse faulting of the East Bay Hills and Mission Hills region, indicating a contractional component to the dextral strike-slip system due to fault geometry [*Aydin and Page*, 1984]. The majority of dextral strike slip in the East Bay is believed to be transferred from the central Calaveras to the Hayward fault in the Mission Hills region [*Andrews et al.*, 1993]. The northern segment continues to the Walnut Creek area where its termination is poorly understood. Here the Calaveras fault appears to form a right stepover with the Concord fault. This is largely based on seismicity from earthquake

swarms during 1970 and 1990 in the stepover region. However, evidence of uplift and the topographic relief across the stepover is not representative of a pull-apart basin [*Smith*, 1992]. An alternative hypothesis suggests that the northern Calaveras fault may transfer slip to the Hayward-Rodgers Creek fault zone or through the East Bay Hills [*Unruh and Lettis*, 1998; *Aydin and Page*, 1984].

[6] Previous estimates of the shallow fault creep and deep slip rate distribution along the Calaveras fault are based largely on surface creep observations, regional slip budgets and geodetic observations. Fault creep, although episodic in nature, is well documented for the southern Calaveras fault in the Hollister area, where average rates approach the estimated long-term slip rate for the southern Calaveras fault [*Galehouse*, 1992]. Alignment arrays in Hollister record surface creep rates from 6.5 to 9.5 mm/yr (J. Galehouse, personal communication, 1999). Although no single array spans all of the fault strands through the town [*Galehouse*, 1992], the sum of measured rates gives a creep rate of 16 mm/yr. A shallow surface slip rate of 15 mm/yr was measured at a power line crossing 13 km north of Hollister [*Savage et al.*, 1979]. Alignment array measurements at the Coyote Lake reservoir suggest a long-term rate of 18 mm/yr (J. Galehouse, personal communication, 1999), including coseismic and postseismic effects of the 1978 Coyote Lake and 1984 Morgan Hill and 1989 Loma Prieta earthquakes. North of Coyote Lake reservoir, the central Calaveras fault enters the Diablo Range and less is known about the slip and creep behavior of the fault, due to inaccessibility. The 1996 Working Group for Northern California Earthquake Potential (WGNCEP) and 1999 Working Group on California Earthquake Probabilities (WG99) adopted 15 ± 3 mm/yr as the long-term geologic slip rate for the southern and central Calaveras fault segments. This value was based on the previously mentioned observations and the allocation of the regional slip budget across the San Andreas fault system [*WGNCEP*, 1996; *WG99*, 1999].

[7] At the transition from the central to northern Calaveras fault, geodetic networks at Grant Ranch and Calaveras Reservoir infer shallow slip rates of 6–7 mm/yr [*Prescott et al.*, 1981]. The small aperture network in Sunol Valley and offset of nearby power transmission towers suggest shallow surface slip rates of about 3 ± 1 mm/yr for the northern Calaveras fault [*Prescott et al.*, 1981; *Prescott and Lisowski*, 1983]. An alignment array approximately 18 km further north that had detected no surface creep from 1981 to 1993, has begun to exhibit creep at 4.5 mm/yr since 1993 (J. Galehouse, personal communication, 1999). *Kelson et al.* [1996] suggest a long-term slip rate of 5 ± 2 mm/yr for the northern Calaveras fault based on paleoseismic investigations. The WGNCEP and WG99 adopted 6 ± 2 mm/yr for the long-term geologic slip rate for the northern Calaveras fault [*WGNCEP*, 1996; *WG99*, 1999].

[8] This widely varying fault behavior makes characterizing seismic hazard on the Calaveras fault difficult. However, the pattern of largely aseismic areas experiencing periodic moderate earthquakes provides us with an opportunity to compare the seismicity and interseismic slip distributions along the fault. Locked regions may be inferred in areas where slip is occurring at rates much lower than the surrounding region or below the long-term geologic slip rate (loading rate) of the fault. If there is a correspondence between the slip deficient regions of the fault and the areas observed by *Oppenheimer et al.* [1990] and *Oppenheimer and Lindh* [1992], then we have two independent lines of evidence suggesting that these regions are locked and accumulating strain. This would allow for a more precise assessment of the seismic hazard presented by the Calaveras fault.

2. Crustal Deformation Measurements Along the Calaveras Fault Zone

[9] The crustal deformation measurements used in this study consist of Geodolite [*Savage and Prescott*, 1973; *Lisowski et al.*, 1991] trilateration data collected by the U.S. Geological Survey (USGS) since 1970 and Global Positioning System (GPS) location data from 1991 to 1998 (Figure 3). We also incorporate two-color laser trilateration survey data for the Mission Hills region from 1995 to 1997 to provide additional coverage for the Calaveras-Hayward fault stepover. Detailed station coordinates, baseline change rates, and GPS station velocities, and a priori slip rate data are included as auxiliary material[1].

2.1. Trilateration Data

[10] Periodic surveys of trilateration networks were conducted by the USGS throughout the San Francisco Bay region from 1972 to 1989 [*Lisowski et al.*, 1991], including lines spanning the Calaveras fault. Several small aperture trilateration networks also span the Calaveras fault. These were located at Hollister (Hollister net), Halls Valley (Grant net), Calaveras reservoir (Calaveras net), Sunol Valley (Veras net) and Pleasanton (Camp Parks net) [*Savage et al.*, 1979; *Prescott et al.*, 1981; *Prescott and Lisowski*, 1983; *Prescott et al.*, 1984]. We use the trilateration data from the Hollister, Calaveras and Grant networks in our modeling to constrain the distribution of shallow slip on the fault. Additionally, we use shallow slip estimates from the Veras and Camp Parks nets, as well as an alignment array rate in San Ramon (J. Galehouse, personal communication, 1999) as a priori slip rates for certain shallow elements on the northern Calaveras fault.

[11] The trilateration data used in the modeling are baseline length change rates (M. Lisowski, personal communication, 1996). Baseline length measurements from different surveys are differenced to calculate a time series of baseline length changes. The average baseline length change rates are calculated by performing a least squares fit to the time series of baseline lengths, assuming that the rate of line length change is constant for each baseline. We use these baseline length change rates in our inversion. Figure 3 shows the trilateration station velocities calculated from the line length change rates and station coordinates using an inner-coordinate solution [*Segall and Mathews*, 1988].

[12] The trilateration data represent the best source of geodetic data for the Calaveras fault, with a time series of almost 20 years. However, during this period two moderate

[1] Auxillary material is available via Web browser or via Anonymous FTP from ftp://ftp.agu.org/append/jb/2002JB001749); subdirectories in the ftp site are arranged by paper number. Information on searching and submitting electronic supplements is found at http://www.agu.org/pubs/esupp_about.html.

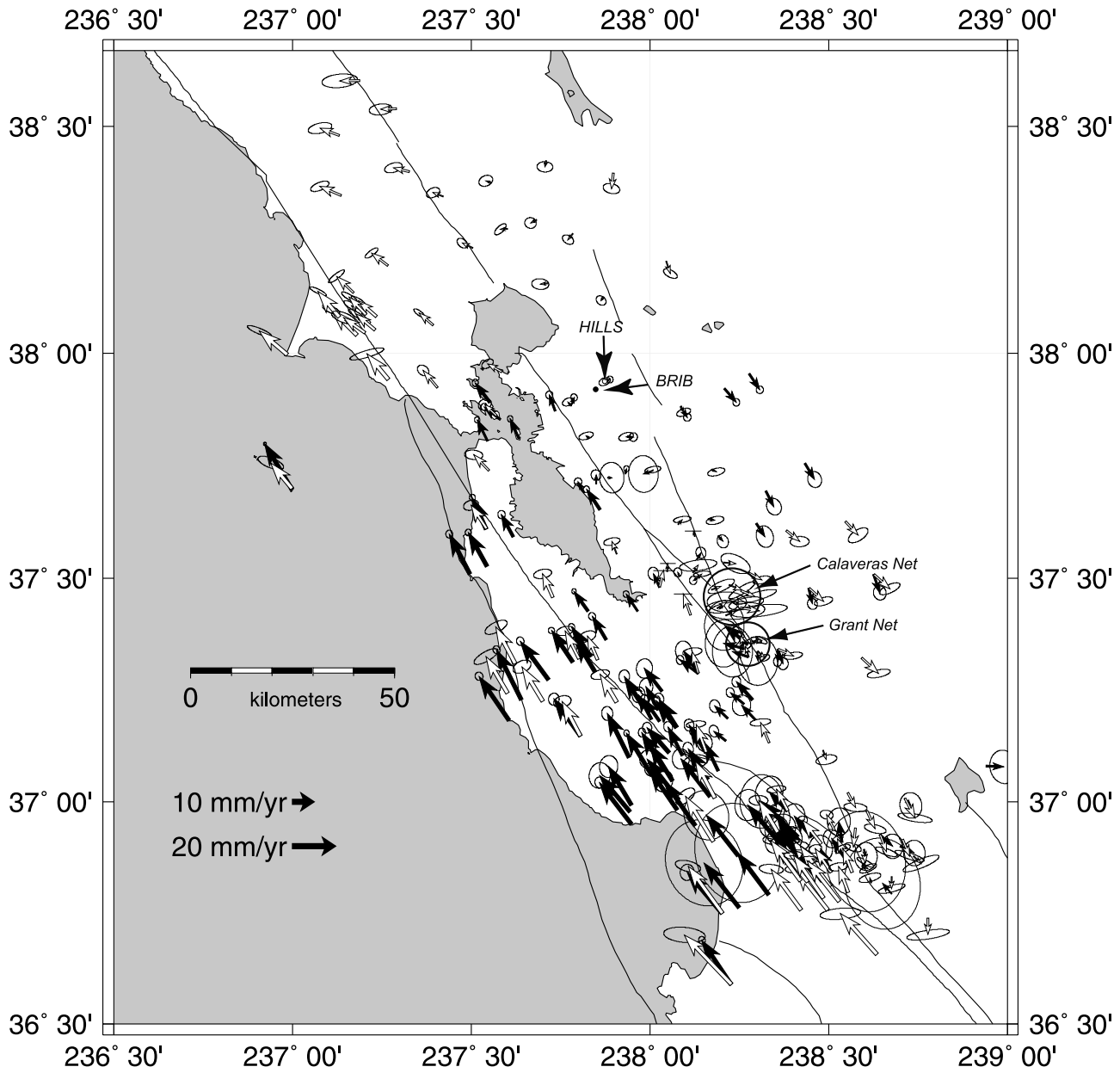

Figure 3. Surface deformation rates used in the study. GPS station velocities for 1990–1998 are shown in solid arrow; open arrows are trilateration station velocities for 1970–1998. Ellipses indicate the 95% confidence range. The trilateration station velocities shown were calculated from the line length change rates and station coordinates using an inner-coordinate procedure that minimizes rotations [*Segall and Mathews*, 1988]. Actual baseline length rate changes were used in the modeling. GPS station velocities calculated relative to station BRIB. Trilateration velocities are relative to station HILLS, located near BRIB.

earthquakes occurred on the Calaveras fault. Since we only want to model the distribution of interseismic slip rates, any coseismic and postseismic effects are detrimental. The coseismic and immediate postseismic transients for the 1979 M_L 5.9 Coyote Lake and 1984 Morgan Hill M_L 6.2 earthquakes have potentially the greatest effect on our modeling. These are removed from the trilateration data by using either preseismic or postseismic observations for rate calculations, based on which data set offers the longest time series [*Lisowski et al.*, 1991]. This does not take into account the effects of long-term postseismic transients. However, any postseismic transients are likely small and short-lived, and are unlikely to effect the longer-term rate estimates [*Lisowski et al.*, 1991].

2.2. GPS Data

[13] The GPS data used for this study include reduced coordinate results from *Bürgmann et al.* [1997], additional regional GPS campaign data collected by UC-Davis and the USGS, and continuous GPS station data from the Bay Area Regional Deformation (BARD) network, spanning period from 1990 to 1998. GPS data were postprocessed to achieve

the necessary level of repeatability. Double-differenced ionosphere-free carrier phase observations are used to estimate station coordinates, tropospheric zenith delays and integer phase ambiguities [*Bürgmann et al.*, 1997]. All of the collected data from the southern Bay Area were processed using the Bernese GPS processing software versions 3.5–4.0, developed at the University of Bern. The continuous data collected through the BARD network were processed with campaign data collected for this project during the same time period. The latest GPS campaign data were also processed at UC-Davis using Bernese GPS software in the months following the data collection. Careful comparisons were made to ensure successful integration of data in our velocity solutions. All BARD data and additional International GPS Service for Geodynamics (IGS) sites in California for these days were included in the processing. A more complete description of our GPS data processing techniques is given by *Bürgmann et al.* [1997].

[14] We also include campaign data collected in 1996 and 1997 along the Calaveras fault, resurveying the Grant network and portions of the Calaveras and Hollister networks to constrain the near-fault deformation (and subsequently, shallow slip distribution). In particular, the reoccupation of the Grant network provides recent information on the transition from the central to northern Calaveras fault. These small aperture networks (<5 km baselines) had been unsurveyed since the mid-1980s, except for one GPS occupation in the early 1990's of the Calaveras network by the USGS.

[15] A transient postseismic signal following the 1989 Loma Prieta earthquake was observed in the surface deformation rates following the event. Only stations within ~30 km of the epicenter were affected and postseismic deformation rates after this event returned to preevent levels by 1993 [*Segall et al.*, 2000]. Therefore we removed GPS data for the affected stations prior to 1993 to account for these transients since they may affect our modeling. After these corrections, we obtained least squares estimates of the relative station velocities along the Calaveras fault from GPS data spanning the period 1990 to 1998 (Figure 3).

2.3. Treatment of Observation Data Uncertainties

[16] Aside from the uncertainties associated with the least squares estimation of deformation rates, we also need to consider the effect of time-correlated noise present in the data. The presence of random walk noise in any time series with infrequent observations requires that we address this additional source of error to our observations. *Langbein and Johnson* [1997] found that the random walk noise averages ~1.3 mm/yr$^{1/2}$, with an additional seasonal noise term that can range as high as 3 mm, but that is usually <0.5 mm. We address this noise by adding a random walk contribution to the data uncertainties. Specifically, we add an amount that is inversely proportional to the square root of the observation time. This approach is simplistic but takes into account the additional uncertainty in the observation data. For the trilateration data, a position uncertainty equal to the 1.3 mm/yr$^{1/2}$ divided by the square root of the number of years of observation for each baseline was used. This provides an estimate of the random walk error baseline that was added to the respective baseline rate uncertainty. For example, a baseline rate from a 6-year time series would have an additional error of 0.53 mm/yr compared to 0.41 mm/yr for a 10-year time series. For the GPS data, a uniform error of (0.58 mm/yr) was incorporated in the data and added to each GPS rate uncertainty based on the random walk noise term for a 5-year period following cessation of the postseismic relaxation signal of the 1989 Loma Prieta earthquake.

3. Model Inversions

[17] We use the horizontal crustal deformation rate measurements to constrain a model of the three-dimensional distribution of interseismic slip rates in the seismogenic zone of the Calaveras fault. We model the horizontal surface displacement rate to be the result of strike-slip motion on vertical dislocations representing the Calaveras fault and the other major faults of the San Andreas system in the San Francisco Bay area. We invert for the interseismic fault slip rates using the surface displacement field and the Green's function relation for surface displacement due to dislocation in a homogeneous, isotropic, elastic half-space [*Steketee*, 1958].

[18] We use the algorithm DIS3D from *Erickson* [1987] to generate the Green's function matrix for the model inversion and an initial fault model developed by *Bürgmann et al.* [1994] with modifications. The modifications consist of adding discretization to the Calaveras, Hayward and San Andreas faults, as well as deleting the Sargent, southern San Gregorio and Rinconada faults. The Sargent fault was deleted due to its proximity to the San Andreas fault and overlapping zones of deformation. Seismic evidence suggests that these faults merge into a single structure at depth [*McLaughlin*, 1990; *Marshall et al.*, 1991]. Thus the San Andreas fault slip rates will include the Sargent fault slip in this area. The southern San Gregorio and Rinconada faults were deleted since they are poorly covered by geodetic data and their contribution to the regional slip budget in the area of interest is minimal.

[19] Geological and seismological information was used to establish fault parameters (i.e., fault geometry, fault segmentation, etc.). We divide most segments into two depth ranges: a seismogenic region from 0 to ~10 km, depending on the fault; and a deep slip zone (>~10 km) with a slip rate at the estimated long-term geologic rate. Some segments are combined to simplify the model and reflect the density of our geodetic data. Table 1 lists the major fault segments and Figure 4 shows the fault segments used in the modeling. Segment boundaries are based on significant changes in strike or fault behavior. The Calaveras fault (including the Paicines fault extension) is specifically represented by the first seven segments listed in Table 1.

[20] We further subdivide the seismogenic range (0–9 km) of the Calaveras fault into discrete ~6 km long by 3 km deep elements (Figure 5a). This discretization of the shallow and seismogenic zones provides for the estimation of the detailed slip rate distribution for comparison with the distribution of microseismicity. We also discretize segments for the Hayward and San Andreas faults that are proximal to the Calaveras fault. A complete listing of all of the fault elements and their geometry is presented in Table 2.

[21] Inversion of geodetic data for fault slip can be unstable and similar surface deformation patterns can be produced by different models with different slip distributions

Table 1. Dislocation Model Segment Endpoints Used to Define the Regional Fault Model[a]

Segment	Southern End	Northern End
Calaveras-Paicines	36°41.47′N, 121°15.02′W	36°49.42′N, 121°23.73′W
Calaveras-Hollister	36°49.42′N, 121°23.73′W	36°55.42′N, 121°26.00′W
Calaveras-Coyote	36°55.42′N, 121°26.00′W	37°07.02′N, 121°33.03′W
Calaveras-Morgan Hill	37°07.02′N, 121°33.03′W	37°21.33′N, 121°43.48′W
Calaveras-Alum Rock	37°21.33′N, 121°43.48′W	37°29.80′N, 121°49.72′W
Calaveras-Sunol	37°29.80′N, 121°49.72′W	37°35.15′N, 121°52.08′W
Calaveras-San Ramon	37°35.15′N, 121°52.08′W	37°48.07′N, 122°00.00′W
Concord	37°54.47′N, 121°59.48′W	38°01.77′N, 122°04.70′W
Green Valley-Southern	38°01.77′N, 122°04.70′W	38°20.53′N, 122°11.68′W
Green Valley-Central	38°20.53′N, 122°11.68′W	38°51.65′N, 122°22.12′W
Green Valley-Northern Central	38°51.65′N, 122°22.12′W	38°57.28′N, 122°28.35′W
Green Valley-Northern	38°57.28′N, 122°28.35′W	38°58.37′N, 122°32.02′W
Greenville-Southern	37°25.33′N, 121°30.20′W	37°35.42′N, 121°35.52′W
Greenville-Northern	37°35.42′N, 121°35.52′W	37°50.17′N, 121°48.52′W
Calaveras-Hayward stepover	37°21.33′N, 121°43.48′W	37°29.73′N, 121°55.32′W
South Hayward-Fremont	37°29.73′N, 121°55.32′W	37°34.85′N, 121°59.37′W
South Hayward	37°34.85′N, 121°59.37′W	37°42.40′N, 122°06.88′W
North Hayward	37°42.40′N, 122°06.88′W	38°06.02′N, 122°26.72′W
Deep Hayward	37°29.73′N, 121°55.32′W	38°06.02′N, 122°26.72′W
Rodgers Creek	38°08.80′N, 122°27.00′W	38°36.70′N, 122°49.90′W
Maacama-Southern	38°35.27′N, 122°42.68′W	38°52.67′N, 123°00.95′W
Maacama-Northern	38°52.67′N, 123°00.95′W	39°00.02′N, 123°03.98′W
Mount Lewis Seismic Trend	37°25.50′N, 121°41.50′W	37°34.00′N, 121°41.50′W
San Andreas-Parkfield	33°00.00′N, 120°30.00′W	36°40.67′N, 121°17.12′W
San Andreas-San Juan Bautista	36°40.67′N, 121°17.12′W	36°51.37′N, 121°32.77′W
San Andreas-Santa Cruz Mountains	36°51.37′N, 121°32.77′W	36°55.92′N, 121°39.53′W
San Andreas-Santa Cruz Mountains	36°55.92′N, 121°39.53′W	37°02.30′N, 121°47.02′W
San Andreas-Loma Prieta	37°02.30′N, 121°47.02′W	37°07.23′N, 121°55.58′W
San Andreas-S. Peninsula	37°07.23′N, 121°55.58′W	37°19.53′N, 122°10.45′W
San Andreas-North Peninsula	37°19.53′N, 122°10.45′W	37°40.07′N, 122°29.42′W
San Andreas-Golden Gate	37°40.07′N, 122°29.42′W	37°54.32′N, 122°40.40′W
San Andreas-Point Reyes	37°54.32′N, 122°40.40′W	38°19.87′N, 123°02.78′W
San Andreas-North Coast	38°19.87′N, 123°02.78′W	38°59.93′N, 123°41.38′W
San Gregorio	36°41.03′N, 122°06.52′W	37°54.32′N, 122°40.40’W

[a]Several segments were discretized into smaller elements used in the modeling (see Table 2).

at depth [i.e., *Savage and Prescott*, 1978]. Additionally, the discretization of the seismogenic zone of the Calaveras fault results in a mixed-determined problem, where some fault elements are overdetermined while others are underdetermined [*Menke*, 1989, pp. 50–52]. Therefore we need to approach the problem with an appropriate analytical method and reasonable constraints to achieve a geologically reasonable solution. Our inversion follows methods used by *Harris and Segall* [1987], *Du et al.* [1992], and *Du and Aydin* [1993] to determine fault slip rates on a discretized model for an underdetermined problem.

[22] We use a least squares inversion penalty function technique with smoothness and positivity constraints to estimate the fault slip from the geodetic data. We employ a technique that minimizes the penalty function, which is the sum of the norm of the residuals from the observed and calculated data and the weighted constraints used for smoothing [*Du and Aydin*, 1993]. From *Du et al.* [1992] the least squares solution is obtained from

$$\mathbf{s}_e = \left(\mathbf{G}^T\mathbf{G} + \alpha^2\mathbf{I} + \beta^2\mathbf{H}^T\mathbf{H}\right)^{-1}\left(\mathbf{G}^T\mathbf{d} + \alpha^2\mathbf{s}_0 + \beta^2\mathbf{H}^T\mathbf{d}_0\right) \quad (1)$$

where $\mathbf{s}_e$ is the estimated slip, $\mathbf{s}_0$ is an initial a priori slip model, α^2 is a damping factor that weights the initial model, $\mathbf{d}$ is the observation data (surface displacement rate field), $\mathbf{d}_0$ is the initial model data (from the initial a priori slip model $\mathbf{s}_o$), $\mathbf{G}$ is the data kernel (the Green's function matrix), $\mathbf{I}$ is the unit matrix, $\mathbf{H}$ is the finite difference approximation of the Laplacian operator ($\nabla^2 = \partial^2/\partial x^2 + \partial^2/\partial z^2$) used in smoothing the slip distribution $\mathbf{s}(x,z)$, and β^2 is the penalty factor that weights the smoothing. For our least squares inversion with smoothing, we use no initial model, thus $\alpha^2 = 0$ and $\mathbf{d}_0 = \mathbf{0}$. Additionally, we apply positivity constraints to the solution (i.e., right-lateral slip only), forcing all values of $\mathbf{s}_e$ to be ≥ 0. Thus the solution becomes:

$$\mathbf{s}_e = \left(\mathbf{G}^T\mathbf{G} + \beta^2\mathbf{H}^T\mathbf{H}\right)^{-1}\left(\mathbf{G}^T\mathbf{d}\right) \quad (2)$$

The a priori slip rate information (see Table 2) from geologic estimates and observed surface creep rates for the fault segments of the regional model is used to prevent instability in the modeling where geodetic data are lacking or poorly distributed. These rates are included as observations in the inversion and are weighted based on the number of observations and their uncertainties. The a priori rates are also used to weakly constrain the deep slip rates. The a priori slip information is based on rate estimates from *WGNCEP* [1996], *WG99* [1999], *Kelson et al.* [1992], and J. Galehouse (personal communication, 1999).

[23] We must carefully consider any constraints that we place on the modeling to avoid biasing the solution. The conditions we impose must be reasonable and not overly restrictive, allowing the model to reflect the observations. The first constraint that we place on the model was a positivity constraint: we restrict the slip to be right-lateral

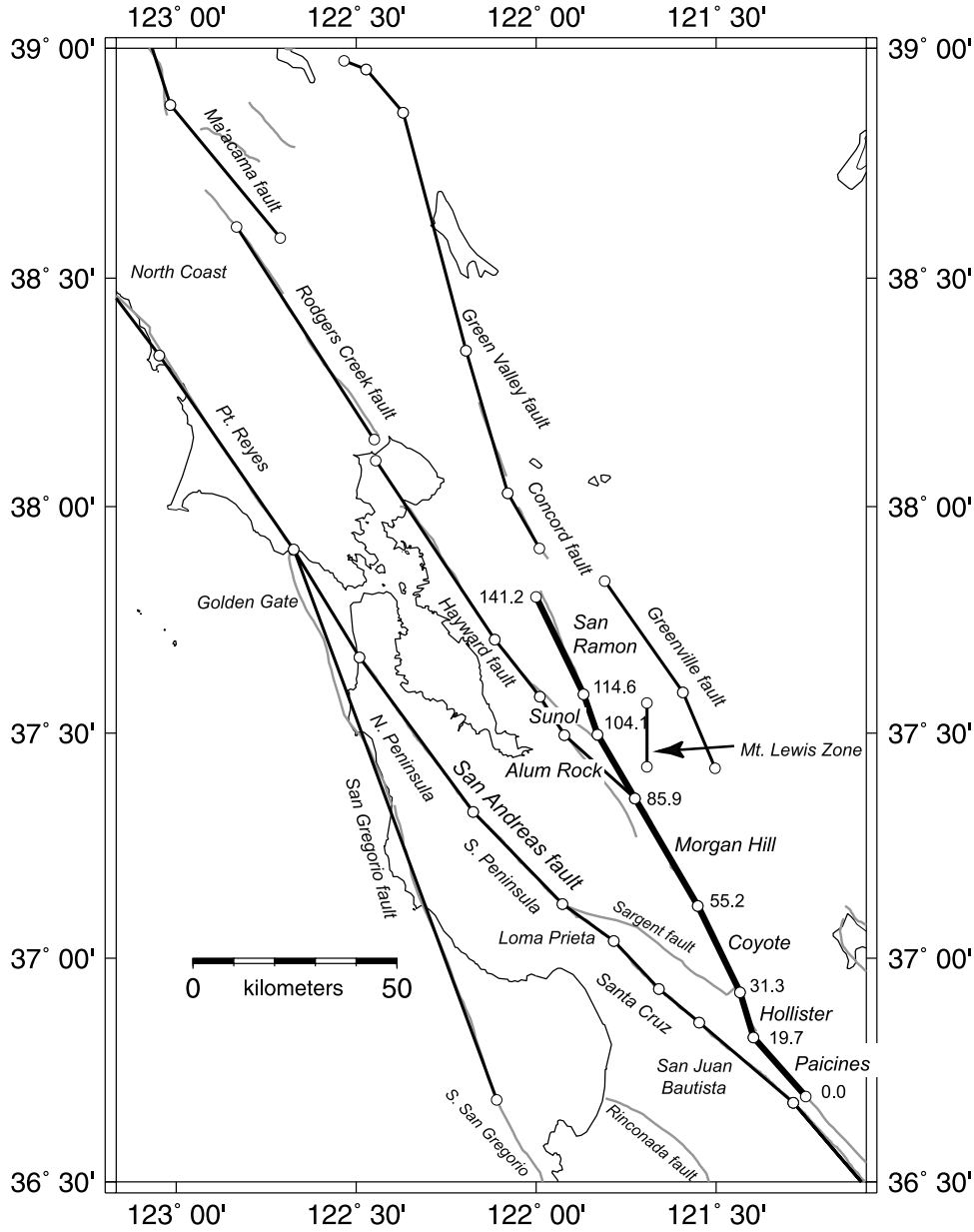

Figure 4. Segmented fault model used for slip inversions. The model segments for the Calaveras fault are shown by heavy black lines with the corresponding segment names used in this paper. Northward fault distances (in km) given at segment endpoints. Other faults used in the model are shown by thin black lines.

only. This is reasonable since the major elements of the San Andreas fault system (of which the Calaveras fault is a part) exhibit strike-slip motion that is exclusively right-lateral (excluding any vertical motion).

[24] Our second constraint was to use a priori slip rate information based on geologic data or measured surface creep. Where surface geodetic data is sparse, the a priori slip values will have a strong influence on the model. Therefore we limit use of these values to only shallow elements where creep is observed and deep elements based on the long-term geologic slip rates, allowing the slip rates in the seismogenic zone to reflect the deformation data.

[25] Third, we imposed a smoothness constraint on the slip rate distribution. This constraint is based on the observation that many natural phenomena, including fault slip distribution, are smooth to a certain degree. The smoothing will affect the slip rate values by "smearing" slip between elements. This will adversely affect the model fit to the observation data, but it will help us deal with the underdetermined elements of our model by linking them to neighboring elements. In order to objectively evaluate the impact of our smoothing, we select the optimal smoothing for the model by finding the value of the smoothing parameter that provides the best balance between the data and model variances. Thus we obtain the smoothest distribution of slip without obscuring the important variations in the observations. We compare the model "roughness" (the square of the norm of the product of the Laplacian operator

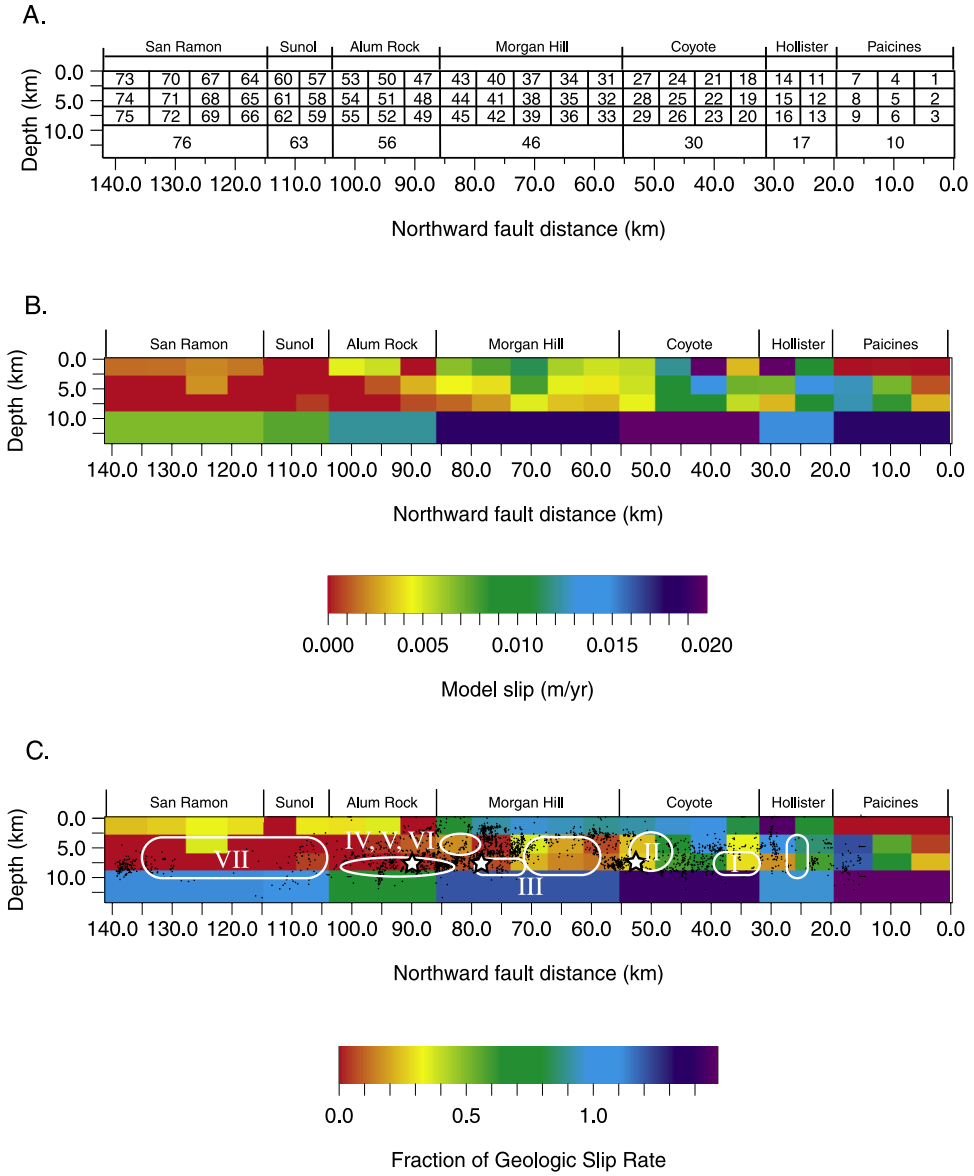

Figure 5. (a) Discretized fault model of the Calaveras fault. Element numbers refer to the inversion results presented in Table 2. The seismogenic zone (0–9 km depth) for each of the seven fault segments was divided into approximately 6 km long by 3 km wide elements. (b) Modeled slip rate distribution for the Calaveras fault with segment boundaries. (c) Comparison of the fraction of the slip rate (ratio of the slip rate to the geologic rates) and microseismicity distribution on the Calaveras fault, showing the correspondence between areas of slip deficit and the locked regions identified by *Oppenheimer et al.* [1990] and *Oppenheimer and Lindh* [1992]. Stars indicate the locations of a northward propagating sequence of three earthquakes from 1979 to 1988.

and the slip matrix [$\|\nabla^2\mathbf{s}\|^2$]) against the weighted sum of the squares of the residuals (WSSR) for different values of the smoothing constraint. We use a wide range of smoothing values from β^2 = 10 to 1000 and look for the smoothing parameter that balances the "trade-off" between the model roughness and WSSR (Figure 6).

4. Model Results

[26] On the basis of the model trade-off curve, the smoothing parameter that provides the optimum balance between model roughness and WSSR is β^2 = 150 (Figure 6). A complete listing of the model results for each of the 142 fault elements is included in Table 2. Increasing the smoothing parameter above β^2 = 200 produces little improvement in model smoothness and significantly increases the data variance. At β^2 = 100, slip rate estimates for several elements in the seismogenic zone exceed 20 mm/yr. These values are unrealistic, considering that the estimated long-term slip rate for that section of the Calaveras fault is 15 ± 3 mm/yr. In general, the final model shows a nonuniform distribution of slip rates in the seismogenic zone on the Calaveras fault (Figure 5b). Although we estimated the slip rates on the Paicines segment, we do not consider it further

Table 2. Fault Model Elements With Corresponding a Priori Slip Values (If Used), Estimated Slip Rates, and Calculated Element Uncertainties

Fault (Segment)	Element	Length, km	Depth, km		Azimuth	Fault Center Coordinates[a] km		A Priori Slip, mm/yr	Modeled Slip, mm/yr	Uncertainty, mm/yr
			Top	Bottom		East	North			
Calaveras fault										
(Paicines segment)	1	6.56	0	3	318.33	54.255	−45.508	none	0.0	0.0
	2	6.56	3	6	318.33	54.255	−45.508	none	1.0	6.6
	3	6.56	6	9	318.33	54.255	−45.508	none	3.0	6.6
	4	6.56	0	3	318.33	49.893	−40.607	none	0.1	5.7
	5	6.56	3	6	318.33	49.893	−40.607	none	6.9	6.3
	6	6.56	6	9	318.33	49.893	−40.607	none	8.4	6.6
	7	6.56	0	3	318.33	45.531	−35.706	none	0.0	0.0
	8	6.56	3	6	318.33	45.531	−35.706	none	12.6	6.0
	9	6.56	6	9	318.33	45.531	−35.706	none	12.5	6.5
	10	19.68	9	3000	318.33	49.893	−40.607	12.0 ± 2.0	17.8	1.8
(Hollister segment)	11	5.8	0	3	342.79	42.491	−30.481	none	10.0	0.9
	12	5.8	3	6	342.79	42.491	−30.481	none	13.4	5.3
	13	5.8	6	9	342.79	42.491	−30.481	none	9.0	6.4
	14	5.8	0	3	342.79	40.772	−24.932	none	33.4	2.4
	15	5.8	3	6	342.79	40.772	−24.932	none	7.0	5.9
	16	5.8	6	9	342.79	40.772	−24.932	none	3.0	6.4
	17	11.62	9	3000	342.79	41.631	−27.707	15.0 ± 2.0	15.0	1.9
(Coyote segment)	18	5.98	0	3	333.83	38.595	−19.476	none	3.1	2.9
	19	5.98	3	6	333.83	38.595	−19.476	none	7.1	5.9
	20	5.98	6	9	333.83	38.595	−19.476	none	5.4	6.4
	21	5.98	0	3	333.83	35.959	−14.112	none	20.3	4.5
	22	5.98	3	6	333.83	35.959	−14.112	none	14.7	6.3
	23	5.98	6	9	333.83	35.959	−14.112	none	10.3	6.5
	24	5.98	0	3	333.83	33.323	−8.748	none	12.0	5.1
	25	5.98	3	6	333.83	33.323	−8.748	none	10.8	6.4
	26	5.98	6	9	333.83	33.323	−8.748	none	9.0	6.6
	27	5.98	0	3	333.83	30.687	−3.385	none	5.5	5.9
	28	5.98	3	6	333.83	30.687	−3.385	none	5.2	6.5
	29	5.98	6	9	333.83	30.687	−3.385	none	4.7	6.6
	30	23.9	9	3000	333.83	34.641	−11.43	15.0 ± 2.0	21.7	1.7
(Morgan Hill segment)	31	6.14	0	3	329.54	27.812	1.944	none	5.1	5.2
	32	6.14	3	6	329.54	27.812	1.944	none	4.2	6.4
	33	6.14	6	9	329.54	27.812	1.944	none	3.0	6.6
	34	6.14	0	3	329.54	24.699	7.238	none	5.9	6.4
	35	6.14	3	6	329.54	24.699	7.238	none	4.7	6.5
	36	6.14	6	9	329.54	24.699	7.238	none	3.3	6.6
	37	6.14	0	3	329.54	21.585	12.531	none	11.2	6.1
	38	6.14	3	6	329.54	21.585	12.531	none	8.0	6.4
	39	6.14	6	9	329.54	21.585	12.531	none	4.8	6.6
	40	6.14	0	3	329.54	18.472	17.825	none	7.7	5.2
	41	6.14	3	6	329.54	18.472	17.825	none	3.9	6.3
	42	6.14	6	9	329.54	18.472	17.825	none	2.4	6.6
	43	6.14	0	3	329.54	15.358	23.119	none	6.5	2.3
	44	6.14	3	6	329.54	15.358	23.119	none	4.5	6.4
	45	6.14	6	9	329.54	15.358	23.119	none	1.4	6.6
	46	30.7	9	3000	329.54	21.585	12.531	15.0 ± 2.0	18.7	1.7
(Alum Rock segment)	47	6.06	0	3	329.45	12.26	28.377	none	0.0	0.0
	48	6.06	3	6	329.45	12.26	28.377	none	3.0	6.3
	49	6.06	6	9	329.45	12.26	28.377	none	0.9	6.6
	50	6.06	0	3	329.45	9.177	33.599	none	5.3	2.7
	51	6.06	3	6	329.45	9.177	33.599	none	1.0	6.3
	52	6.06	6	9	329.45	9.177	33.599	none	0.0	0.0
	53	6.06	0	3	329.45	6.094	38.822	none	4.7	2.1
	54	6.06	3	6	329.45	6.094	38.822	none	0.0	0.0
	55	6.06	6	9	329.45	6.094	38.822	none	0.0	0.0
	56	18.2	9	3000	329.45	9.177	33.599	15.0 ± 3.0	12.2	2.5
(Sunol segment)	57	5.22	0	3	340.51	3.68	43.898	none	0.0	0.0
	58	5.22	3	6	340.51	3.68	43.898	none	0.0	0.0
	59	5.22	6	9	340.51	3.68	43.898	none	0.6	6.6
	60	5.22	0	3	340.51	1.935	48.827	none	0.0	0.0
	61	5.22	3	6	340.51	1.935	48.827	none	0.0	0.0
	62	5.22	6	9	340.51	1.935	48.827	none	0.0	0.0
	63	10.46	9	3000	340.51	2.808	46.362	7.5 ± 2.0	7.6	1.9

Table 2. (continued)

Fault (Segment)	Element	Length, km	Depth, km		Azimuth	Fault Center Coordinates[a] km		A Priori Slip, mm/yr	Modeled Slip, mm/yr	Uncertainty, mm/yr
			Top	Bottom		East	North			
(San Ramon segment)	64	6.66	0	3	334.02	−0.395	54.284	1.5 ± 1.0	1.7	0.9
	65	6.66	3	6	334.02	−0.395	54.284	none	0.0	0.0
	66	6.66	6	9	334.02	−0.395	54.284	none	0.0	0.0
	67	6.66	0	3	334.02	−3.311	60.268	1.5 ± 1.0	2.0	1.0
	68	6.66	3	6	334.02	−3.311	60.268	none	2.3	5.7
	69	6.66	6	9	334.02	−3.311	60.268	none	0.0	0.0
	70	6.66	0	3	334.02	−6.226	66.252	1.5 ± 1.0	1.5	1.0
	71	6.66	3	6	334.02	−6.226	66.252	none	0.0	0.0
	72	6.66	6	9	334.02	−6.226	66.252	none	0.0	0.0
	73	6.66	0	3	334.02	−9.141	72.237	1.5 ± 1.0	1.5	1.0
	74	6.66	3	6	334.02	−9.141	72.237	none	0.0	0.0
	75	6.66	6	9	334.02	−9.141	72.237	none	0.0	0.0
	76	26.62	9	3000	334.02	−4.768	63.26	6.0 ± 2.0	6.7	1.7
Concord fault	77	15.52	0	3	330.49	−13.642	93.82	3.0 ± 1.0	3.0	1.0
	78	15.52	15	3000	330.49	−13.642	93.82	6.0 ± 2.0	7.7	1.9
Green Valley fault	79	36.16	0	3	343.73	−22.527	117.924	4.0 ± 1.0	3.6	0.9
	80	36.16	10	3000	343.73	−22.527	117.924	6.0 ± 2.0	8.8	1.6
	81	59.48	0	3	345.44	−35.065	164.064	4.0 ± 1.0	3.8	1.0
	82	59.48	10	3000	345.44	−35.065	164.064	6.0 ± 2.0	10.2	1.7
	83	13.74	0	3	319.26	−47.025	198.06	4.0 ± 1.0	3.9	1.0
	84	13.74	10	3000	319.26	−47.025	198.06	6.0 ± 2.0	5.6	1.9
	85	5.68	0	3	290.82	−54.162	204.277	4.0 ± 1.0	3.9	1.0
	86	5.68	10	3000	290.82	−54.162	204.277	6.0 ± 2.0	5.3	1.9
Greenville fault	87	20.28	12	3000	336.99	29.474	42.497	2.0 ± 1.0	1.9	1.0
	88	33.38	12	3000	324.85	15.904	65.471	2.0 ± 1.0	2.0	1.0
Calaveras-Hayward	89	23.42	0	3	311.56	5.038	33.534	none	6.2	2.5
Slip Transition	90	23.42	3	12	311.56	5.038	33.534	none	1.5	3.5
	91	23.42	12	3000	311.56	5.038	33.534	none	8.4	1.8
Hayward fault	92	11.2	0	3	327.75	−6.712	46.039	9.0 ± 2.0	4.6	0.9
	93	11.2	3	6	327.75	−6.712	46.039	5.0 ± 2.0	0.0	0.0
	94	11.2	6	9	327.75	−6.712	46.039	none	0.0	0.0
	95	11.2	9	12	327.75	−6.712	46.039	none	0.0	0.0
	96	17.82	0	3	321.64	−15.227	57.757	none	0.0	0.0
	97	17.82	3	6	321.64	−15.227	57.757	none	0.0	0.0
	98	17.82	6	9	321.64	−15.227	57.757	none	0.0	0.0
	99	17.82	9	12	321.64	−15.227	57.757	none	0.0	0.0
	100	52.42	0	3	326.45	−35.243	86.587	none	4.2	2.0
	101	52.42	3	6	326.45	−35.243	86.587	none	4.7	5.2
	102	52.42	6	9	326.45	−35.243	86.587	none	5.0	5.8
	103	52.42	9	12	326.45	−35.243	86.587	none	4.1	6.1
Deep Hayward	104	81.38	12	3000	325.58	−26.728	74.869	9.0 ± 2.0	16.5	1.4
Rodgers Creek fault	105	61.28	10	3000	327.39	−66.621	139.385	9.0 ± 2.0	14.7	1.6
Ma'acama fault	106	41.52	0	3	320.85	−85.748	178.643	6.0 ± 1.0	5.8	1.0
	107	41.52	10	3000	320.85	−85.748	178.643	9.0 ± 2.0	11.0	1.9
	108	14.24	0	3	342.77	−100.96	201.539	6.0 ± 1.0	5.9	1.0
	109	14.24	10	3000	342.77	−100.96	201.539	9.0 ± 2.0	9.1	1.9
Mt. Lewis Zone	110	15.72	10	3000	359.89	16.703	41.34	none	11.1	4.3
San Andreas	111	108.6	0	10	318.78	89.088	−90.282	30.0 ± 2.0	28.2	1.8
(central California)	112	537.22	10	3000	319.42	228.045	−253.438	34.0 ± 2.0	46.8	1.6
San Andreas fault	113	6.14	0	3	310.16	50.963	−47.459	12.0 ± 1.0	11.6	1.0
(San Juan Bautista)	114	6.14	3	6	310.16	50.963	−47.459	none	0.0	0.0
	115	6.14	6	9	310.16	50.963	−47.459	none	0.0	0.0
	116	6.14	9	12	310.16	50.963	−47.459	none	1.2	6.6
	117	6.14	0	3	310.16	46.273	−43.502	10.0 ± 1.0	9.8	1.0
	118	6.14	3	6	310.16	46.273	−43.502	none	1.9	6.3
	119	6.14	6	9	310.16	46.273	−43.502	none	2.8	6.6
	120	6.14	9	12	310.16	46.273	−43.502	none	3.0	6.6
	121	6.14	0	3	310.16	41.582	−39.544	5.0 ± 1.0	5.2	1.0
	122	6.14	3	6	310.16	41.582	−39.544	none	2.7	5.9
	123	6.14	6	9	310.16	41.582	−39.544	none	2.1	6.5
	124	6.14	9	12	310.16	41.582	−39.544	none	2.5	6.6
	125	6.14	0	3	310.16	36.892	−35.586	none	14.3	1.2
	126	6.14	3	6	310.16	36.892	−35.586	none	7.5	5.7
	127	6.14	6	9	310.16	36.892	−35.586	none	4.7	6.4
	128	6.14	9	12	310.16	36.892	−35.586	none	2.8	6.6
	129	6.14	0	3	310.16	32.202	−31.628	none	12.2	1.5
	130	6.14	3	6	310.16	32.202	−31.628	none	14.1	5.1
	131	6.14	6	9	310.16	32.202	−31.628	none	10.1	6.4
	132	6.14	9	12	310.16	32.202	−31.628	none	5.6	6.6
	133	30.68	12	3000	310.16	41.582	−39.544	14.0 ± 2.0	18.7	1.8

Table 2. (continued)

Fault (Segment)	Element	Length, km	Depth, km		Azimuth	Fault Center Coordinates[a] km		A Priori Slip, mm/yr	Modeled Slip, mm/yr	Uncertainty, mm/yr
			Top	Bottom		East	North			
(Santa Cruz Mountains)	134	13.14	15	3000	309.81	24.809	−25.441	14.0 ± 2.0	14.8	1.9
	135	16.24	15	3000	316.58	14.178	−15.333	14.0 ± 2.0	15.2	1.9
(Loma Prieta Area)	136	15.66	15	3000	305.62	2.233	−4.874	14.0 ± 2.0	15.3	1.9
(South Peninsula)	137	31.66	15	3000	315.94	−15.139	11.061	17.0 ± 2.0	17.6	1.7
(North Peninsula)	138	47.12	15	3000	323.75	−40.076	41.433	17.0 ± 2.0	18.2	1.6
(Golden Gate)	139	30.78	15	3000	328.76	−61.989	73.592	17.0 ± 2.0	18.2	1.8
(Point Reyes)	140	57.28	15	3000	325.67	−86.125	110.405	25.0 ± 2.0	28.7	1.7
(North Coast)	141	92.26	15	3000	323.45	−129.75	171.114	25.0 ± 2.0	27.7	1.8
San Gregorio fault	142	144.3	12	3000	339.95	−45.235	19.009	4.0 ± 2.0	3.7	1.4

[a]Fault center coordinates with respect to regional model center at 37°02.40′N, 121°52.80′W.

since its proximity and parallel trend to the San Andreas fault make distinguishing slip at depth unlikely. Additionally, we do not discuss the deep elements (≥9 km depth) further, accepting the long-term geologic rate used as a priori information for the modeling. The modeled deep slip rates essentially remain unchanged from the a priori values, with only the Hayward fault, Rodgers Creek fault and creeping San Andreas fault in central California departing significantly from these the a priori values (which will be addressed later).

[27] The distribution of slip rates on the Hollister segment indicates a zone of decreased slip ~6–9 km deep. Slip rates on elements 15 and 16 are 3.0 and 7.0 mm/yr, respectively. These are considerably less than the long-term geologic rate (15 ± 3 mm/yr) and observed surface creep rates near the town of Hollister. However, element 14 has a slip rate of 33.4 mm/yr, which exceeds the observed creep rate of 15 mm/yr in the town of Hollister [*Galehouse*, 1992; *Savage et al.*, 1979]. This high value is likely due to remaining stability problems in the model inversion. The Coyote segment shows regions of possible slip deficit, with elements 18–20 and 27–29 having slip values from 3.7 to 7.1 mm/yr (average of 5.3 mm/yr). This average rate is 35% of the estimated long-term geologic slip rate of 15 mm/yr [*Kelson et al.*, 1992]. Elements 21–26 have slip rates that are in closer agreement with the long-term geologic rate (average of 12.9 mm/yr).

[28] Further north, the model suggests a large portion of the seismogenic zone of the Morgan Hill segment is slipping at rates that are below the long-term geologic slip rate of 15 mm/yr [*Kelson et al.*, 1992]. Of the 15 seismogenic zone elements, all have slip rate estimates that are below 12 mm/yr, and 8 are less than 5 mm/yr. The model also suggests an absence of slip in the seismogenic zone of the Alum Rock, Calaveras reservoir and Sunol-San Ramon segments. The shallow elements for these creeping segments reflect the a priori rates provided as observations obtained from small aperture networks [*Prescott et al.*, 1981; *Prescott and Lisowski*, 1983] and alignment arrays (J. Galehouse, personal communication, 1999). The model suggests that virtually no slip is occurring in the seismogenic zone, except for shallow slip near the Calaveras reservoir (elements 50 and 53) of 5.0 mm/yr and on the San Ramon segment (elements 67 and 68) of 2.1 mm/yr.

[29] Looking beyond the Calaveras fault to the other faults of the regional model, we find general agreement with accepted fault slip rates in most cases. The most notable characteristic of the model is that several deep slip values are higher than the accepted geologic slip rates, although in most cases well within the 95% confidence range. Exceptions to this include the San Andreas fault in central California (likely due to the absence of observation data spanning the fault), the Hayward fault, and Rodgers Creek fault. A comparison of the regional slip budget of 40 mm/yr [*WG99*, 1999] in the SFBR to the preferred model shows that the best fit is in the southern region of the model and is worst in the north. The southern profile, including the San Gregorio, San Andreas and Calaveras faults has a regional slip rate sum of 37.4 ± 2.9 mm/yr. The central profile, including the San Gregorio, San Andreas, Hayward and northern Calaveras faults, has a regional slip rate sum of 45.9 ± 3.1 mm/yr. The northern profile, including the San Andreas, Rodgers Creek and Green Valley faults, has a regional slip rate sum of 53.7 ± 2.9 mm/yr. These rates are not in agreement with the regional geologic slip rate budget. *Prescott et al.* [2001] observed similar disagreement with the geologic rates due to a lack of far-field geodetic data in the northern SFBR and locking depth selection. In particular, *Prescott et al.* [2001] found inconsistencies between slip rate on the San Andreas fault and the locking depth defined by seismicity distribution. This was also observed

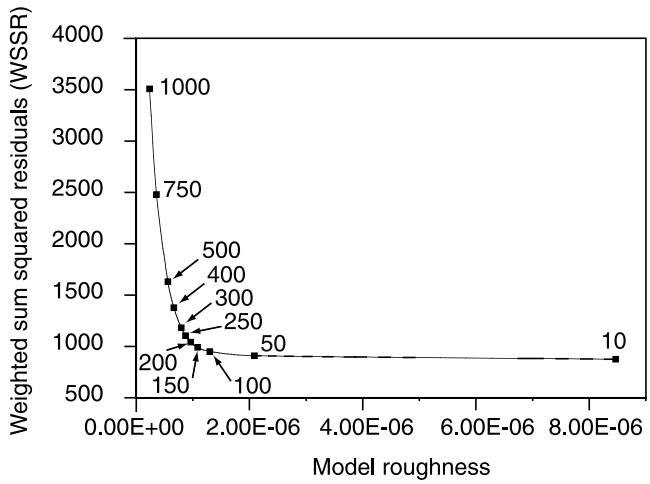

Figure 6. Inversion trade-off curve comparing the model roughness and the weighted sum of the squared residuals (WSSR) for various smoothing values. Optimum values of the smoothing parameter range from 100 to 200. Note the decrease in improvement of roughness for smoothing values greater than 200.

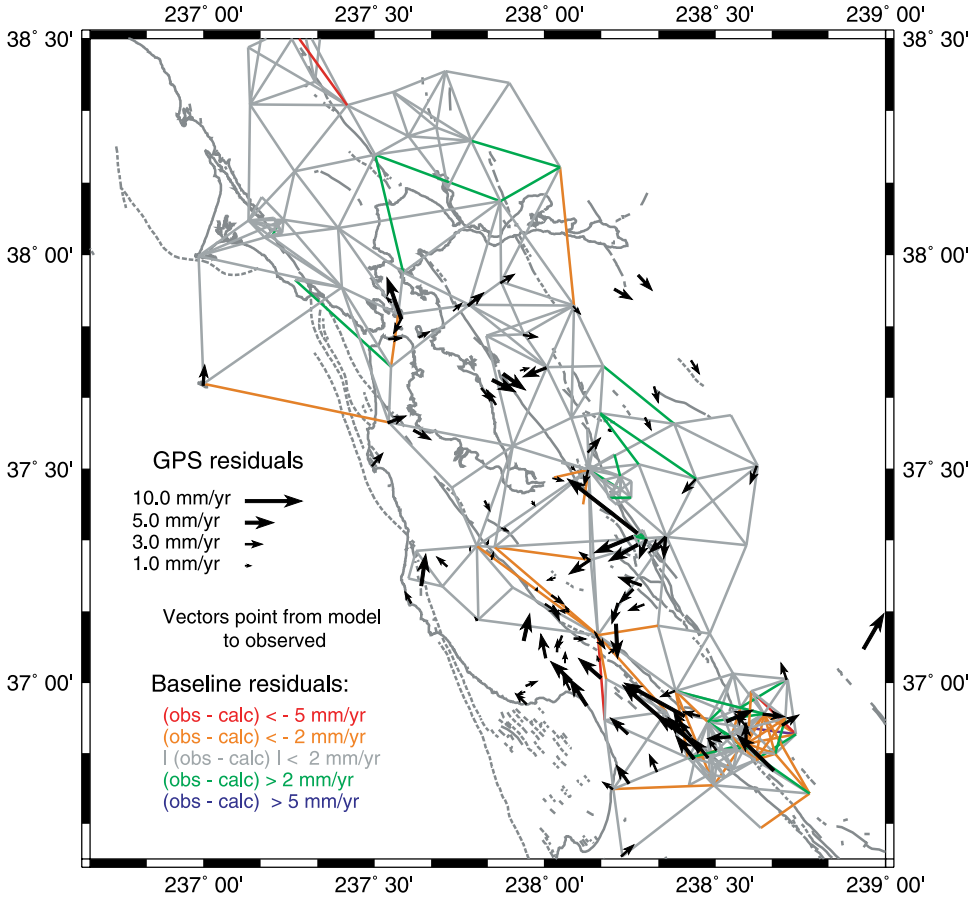

Figure 7. Residuals for preferred fault slip model. The color of the baselines indicates the magnitude and sign of the residual. GPS residuals represented by vectors that indicate the magnitude and direction of the station motion not fit by the model. Note misfit in the southeastern region due to the complex deformation pattern of the San Andreas-Calaveras fault triple junction.

by *Freymueller et al.* [1999]. Regardless, these far-field aspects of the regional model do not affect the local (and shallow) patterns of slip inferred on the Calaveras fault.

5. Evaluation of Model Quality

[30] Our modeling is a mixed-determined problem and the area of interest is largely underdetermined. This is problematic, so we must consider if the model parameters in the study area are adequately illuminated. That is, are the results of our model reasonable and of sufficient quality to confidently estimate the fault slip rates within the seismogenic zone of the Calaveras fault? First, we consider the estimated model error obtained from the weighted design matrix (the original matrix **G** combined with the Laplacian filter **H** in equation (2)). The model covariance matrix is calculated from the following:

$$\mathrm{cov}_u\ \mathbf{m} = \left(\mathbf{G}^{\mathrm{T}}\mathbf{G} + \beta^2\mathbf{H}^{\mathrm{T}}\mathbf{H}\right)^{-1}\left(\left(\mathbf{G}^{\mathrm{T}}\mathbf{G} + \beta^2\mathbf{H}^{\mathrm{T}}\mathbf{H}\right)^{-1}\right)^{\mathrm{T}} \quad (3)$$

From this, the model uncertainty is calculated from the square root of the diagonal terms of the model covariance matrix. Table 2 shows the model results with the uncertainties. Again, we focus on the discretized elements of the Calaveras fault, since this is the primary area of focus for this study. The model uncertainties average ~6 mm/yr. At first, this result would appear unsettling, since many of the slip rate values we obtained are comparable to their uncertainty estimates. However, this result is not unexpected, since the solution in this region is largely underdetermined. We can extract valuable information from these results despite these uncertainties, recognizing that they do represent weighted averages for the true values.

[31] We can also examine other aspects of the modeling to evaluate its quality. First, we can examine the fit of the model with the crustal deformation measurements. Overall, there is good agreement between the estimated station velocities of the model and the geodetic observation data. Figure 7 shows the residuals (observed less modeled rates) for the preferred model. Most of the residuals display a random pattern, indicating that modeling is not introducing a systematic deviation from the observational data. However, some patterns are visible in the residuals. The GPS and trilateration data both suggest higher rates in the northeasternmost portion of the regional model, as well as along the San Andreas fault from San Juan Bautista to Loma Prieta. Although modeling predicts velocities with less northwesterly motion than the observed velocities along the San Andreas fault in the San Juan Bautista area and the Santa Cruz mountains, most of the predicted velocities are within the 95% confidence intervals of the observed velocities. The

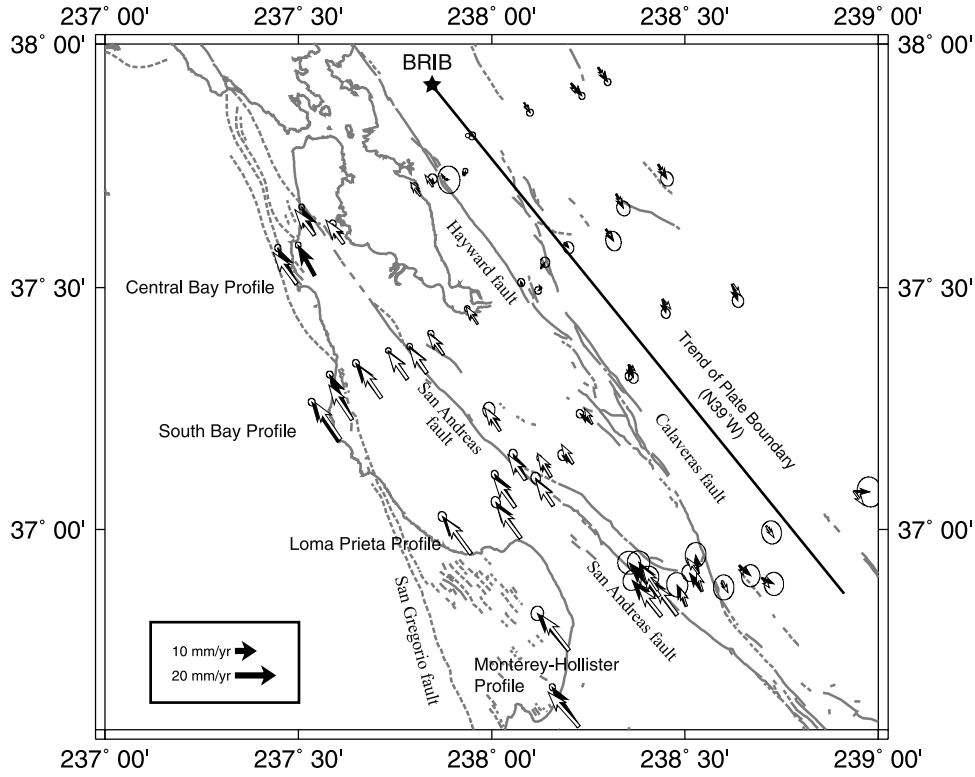

Figure 8. Observed and predicted model velocities for four U.S. Geological Survey profiles. Observed velocities and their 95% confidence ellipses are shown in black. Model-predicted velocities shown in white. All velocities are relative to station BRIB. Line trending S39°E from BRIB denotes the plate boundary-parallel "zero" axis used in profile velocity comparisons.

trilateration baseline rates are generally well modeled, with the exception of the San Andreas-Calaveras fault triple junction near Hollister. Trilateration data east of Hollister is exhibits notable misfit, likely due to the presence of multiple strands of the Calaveras fault [*Galehouse*, 1992] in the Hollister area. The misfit suggests higher rates of slip across the triple junction region than modeled. However, the modeled rates show generally good fit to the GPS data. This misfit is not totally unexpected. Past studies suggest considerable internal deformation and a complex slip distribution within this region [*Savage et al.*, 1979; *Matsu'ura et al.*, 1986], as observed in the creep rates on the multiple strands of the Calaveras fault through downtown Hollister [*Galehouse*, 1992].

[32] Overall, the preferred model gives a $\chi^2 = 1.77$ (WSSR divided by degrees of freedom), indicating that the model provides a good fit to the observational data while achieving a realistic distribution of subsurface slip rates. We performed additional tests, using an undiscretized Calaveras fault model (same segment boundaries). The discretized model has a lower WSSR at 990 compared to the undiscretized model at 1125, but has a comparable $\chi^2 = 1.76$. The discretized model produced a lower model roughness of 1.09×10^{-6} compared to 7.53×10^{-5} for the undiscretized model. While the discretization of the Calaveras fault does not lead to much improved statistical fits to the total data set, the added fault elements improve the fit to sites in the closer vicinity of the fault.

[33] A comparison of the predicted surface velocities with the observed velocities also provides a means to assess the model quality. Several USGS profiles span the San Andreas fault system (Figures 8 and 9), trending roughly perpendicular to the fault system and the distributed plate boundary. A comparison between the observed and predicted plate boundary-parallel velocities for four USGS profiles reveals a qualitatively good fit between the modeled and observed data.

[34] Although some of the modeled velocities differ from the observed velocities at the one standard deviation, most are within the 95% confidence range (including the random walk error) of the observed velocities. The observed and modeled profiles differ most near the edges of the model, indicating that the lack of far-field observations limits the model's ability to constrain the regional slip budget, as well as in regions where the deformation is complex (as previously seen in the residuals). Misfit also occurs where there is pronounced scatter in the observation data (i.e., near the Hayward fault in Figure 9d).

[35] Next, we examine the impact of the data limitations and the effect of the smoothing on the resolution of our model. Since the discretization of the seismogenic region will result in locally more parameters than observations, we use positivity constraints and smoothing to reduce the model instability. The smoothing results effectively "smears" the slip distribution among neighboring fault elements, resulting in slip rate values that have contributions from neighboring elements. Our selection of $\beta^2 = 150$ as the optimal model is based on the model trade-off between the fit to the observation data and the model roughness and the realistic distribution of slip rate. We compute the resolution matrix using the methodology of *Du and Aydin* [1993], *Du et al.* [1992], and

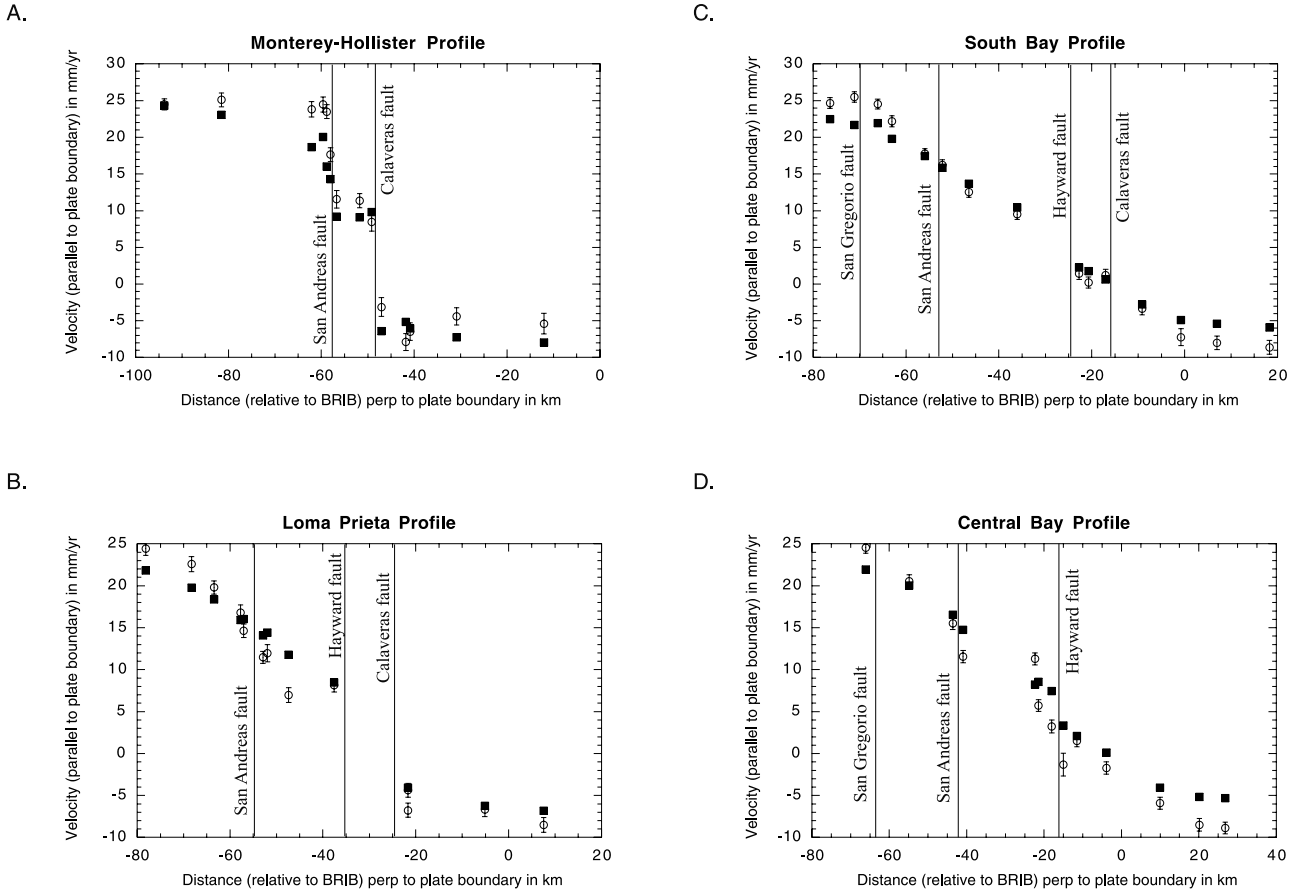

Figure 9. Observed and predicted plate boundary-parallel and perpendicular velocities for four U.S. Geological Survey profiles. These profiles are shown in Figure 8: (a) Hollister profile; (b) Santa Cruz Mountain profile; (c) South Bay profile; and, (d) Central Bay profile. Open circles show the observed plate boundary-parallel velocities, with error bars representing one standard deviation for boundary-parallel motion, including the random walk error term. Black squares show the predicted plate boundary-parallel velocities. Vertical lines show major faults crossing the profile. In general, the model misfit is good in the central model region and poor at the outer edges of the model or in zones of complex deformation.

Harris and Segall [1987]. We fix unit slip on a particular element and zero slip on all other elements and run a forward model to produce synthetic surface displacement data. We then back substitute the synthetic surface displacement rates, assigning the data uncertainties used in the modeling, and invert the synthetic data to recover the fault slip rate distribution. This procedure is repeated for each of the 142 fault elements of the model and assembled into the resolution matrix. A perfectly resolved element should recover unit slip on each element. However, the use of smoothing and mixed-determined nature of the profile means that the recovered fault slip rates will be smeared on nearby elements. An examination of the diagonal elements of the resolution matrix (Figure 10a) for the Calaveras fault shows strong model resolution from 0–3 km depth where geodetic data are present. The diagonal elements are weaker for shallow fault elements where the geodetic data are sparse, as well as for the short-length deep elements, especially from 6–9 km. As expected, where faults are closely spaced, there is trade-off with neighboring faults. An example of this can be seen in Figure 10b, where element 111 (the shallow creeping San Andreas fault south of Hollister), shows a resolution spread to neighboring faults. However, the strength of the model resolution largely remains on the particular element (at the diagonal) or is distributed to the immediate vicinity (around the matrix diagonal).

[36] To further test the model resolution and the effect of the smoothing, we ran another inversion in which we assigned zero slip to the elements of the Calaveras fault that we interpret as being "locked" and assigned the full geologic slip rate to the surrounding elements. We used the preferred smoothing factor for the inversion and compared the resulting slip pattern with the input slip pattern to see the amount of smearing that occurred. The comparison yielded no significant deviation between the input and output slip rate models, indicated that the amount of "smearing" occurring between elements is minimal. Therefore we feel that our model reasonably reflects the slip rate distribution within the seismogenic zone.

6. Discussion

[37] *Oppenheimer et al.* [1990] suggested that the central Calaveras fault exhibits microseismicity along creeping

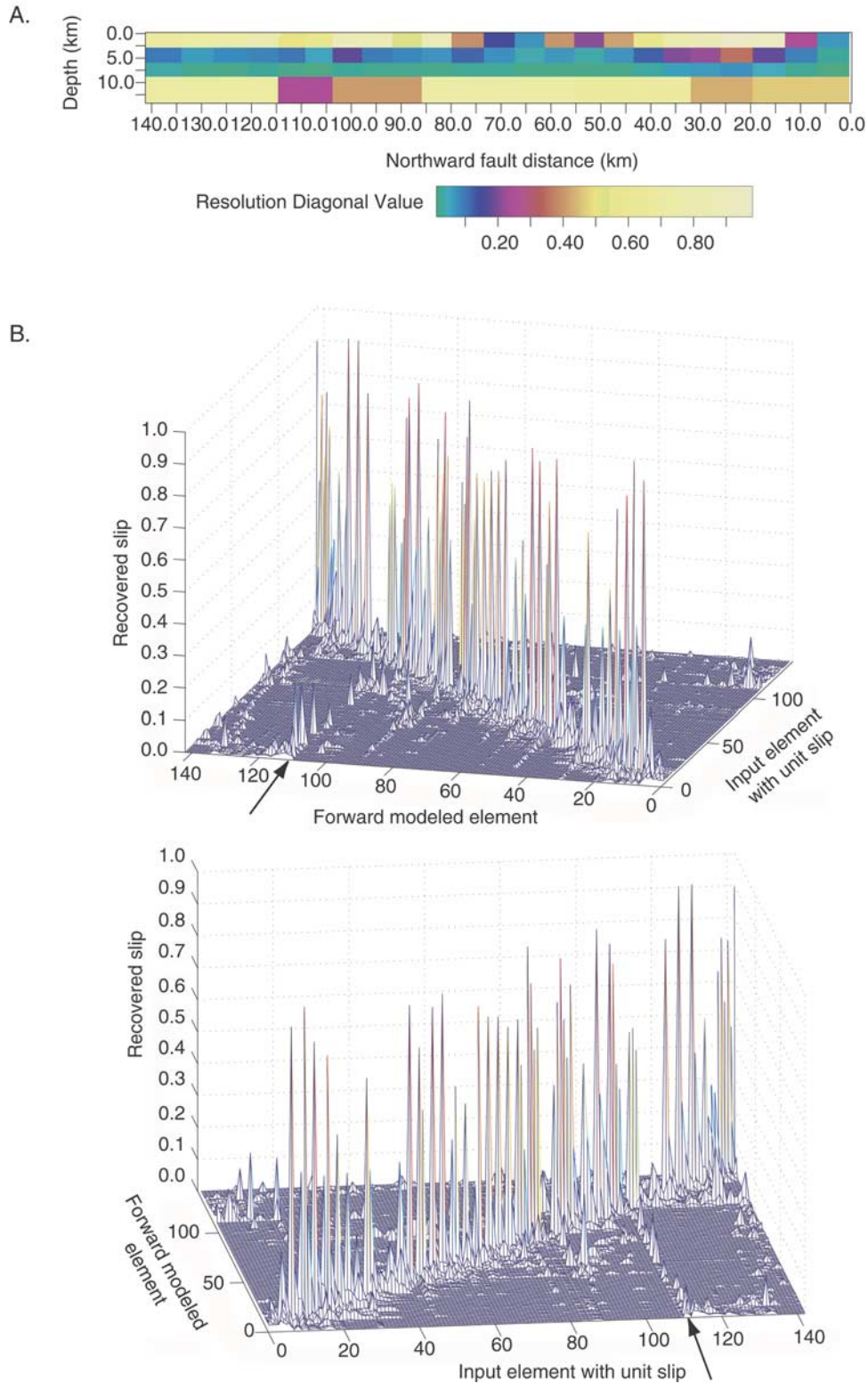

zones at depths from 4 to 10 km and that areas lacking microseismicity are locked and fail during moderate ($M_L > 5$) earthquakes. *Oppenheimer et al.* [1990] and *Oppenheimer and Lindh* [1992] identified seven areas on the central and northern segments of the Calaveras fault that may be locked and accumulating interseismic strain. If this is the case, then there should be a slip rate deficit within these areas. This leads to the following questions: Does our model slip rate distribution agree with the distribution of microseismicity along the fault? Do moment accumulation estimates agree with historical seismicity? In the following discussion, we use catalog earthquake locations for $M \geq 1.5$ events measured by the Northern California Seismic Network that are archived at the Northern California Earthquake Data Center.

Table 3. Seismic Moment and Moment Magnitude Estimates Based on Model Slip Deficit, Fault Area, and Characteristic Event Recurrence Times

Region	Fault Area, km^2	Deficit, mm/yr	Recurrence, years	Moment, dyn cm	Magnitude
Coyote Lake 1979 (II)	36	10.0	80	8.6×10^{24}	5.9
Coyote (I) San Felipe Lake	36	8.7	80	7.6×10^{24}	5.9
Morgan Hill 1984	90	11.0	73	2.3×10^{24}	6.2
Morgan Hill (III)	128	11.0	40	1.8×10^{25}	6.1
Morgan Hill (III)	128	11.0	100	4.3×10^{25}	6.4
Alum Rock 1988 (IV)	18	5.0	45	1.3×10^{24}	5.4
Alum Rock 1996 (V)	18	5.0	40	1.2×10^{24}	5.3
Alum Rock (IV, V, VI)	64	5.0	80	7.8×10^{24}	5.9
Alum Rock (IV, V, VI)	64	5.0	150	1.5×10^{25}	6.1
North of Alum Rock (IV-VII)	306	6.0	150	8.4×10^{25}	6.6
Entire North Calaveras (VII)	216	6.0	150	5.9×10^{25}	6.5
Entire North Calaveras (VII)	216	6.0	550	2.2×10^{26}	6.9
Hollister	36	10.0	50	5.5×10^{24}	5.8

Events for the period 1970–1998 were used for the southern Calaveras fault, 1990–1999 for the central Calaveras fault, and 1970–1998 for the northern Calaveras fault. Different time periods were used since seismicity is markedly less frequent on the southern and northern segments than the central segment of the fault, and we wanted a similar number of hypocenters for comparison. We also calculate seismic moment (see Table 3) for each region of slip deficit corresponding to aseismic areas, using estimated characteristic earthquake recurrence intervals from *Oppenheimer et al.* [1990] and *Kelson et al.* [1996].

[38] The Coyote segment shows two distinct regions of slip deficit that generally correspond to regions I and II of *Oppenheimer et al.* [1990] (Figure 5c). The seismogenic elements 19–20 and 28–29 have slip rate values suggesting an accumulating deficit in these regions. The other seismogenic elements have slip rates that, for the most part, approach the long-term geologic slip rate and suggest that it is likely freely slipping through the seismogenic zone in these regions. Region I was the site of a 1949 M_L 5.2 event. On the basis of an average slip deficit of 8.7 mm/yr for elements 18 and 19 and a recurrence time of 80 years, a M_L 5.9 event is estimated (Table 3). This is also similar to an estimated $\sim M_L$ 6.0 event in 1897 that occurred near region I [*Oppenheimer et al.*, 1990]. Additionally, *Kelson et al.* [1998] have found paleoseismological evidence for multiple large magnitude (at least three discrete) events at San Ysidro Creek, near region I at the southern end of the Coyote segment based on offset stream channels. The 1979 M_w 5.9 Coyote Lake event was located in region II, corresponding to model elements 28 and 29. Moment calculations based on an average slip deficit of 10 mm/yr for these elements and an estimated recurrence time of 80 years [*Oppenheimer et al.*, 1990] provide for a M_w 5.9 event, which is in agreement with the 1979 event. Therefore we find agreement between our model results, the distribution of microseismicity, and the historical and paleoearthquake occurrence.

[39] The Morgan Hill segment has the highest rate of microseismicity of all segments of the Calaveras fault, with some regions exhibiting sparse seismicity while other regions show distinct bands of seismicity. *Oppenheimer et al.* [1990] combined several areas that are devoid of microseismicity into region III. *Schaff et al.* [2002] used a waveform cross correlation and double-difference technique to obtain precise relocations of seismicity from 1984 to 1997 of this region. They were able to resolve highly organized structures much better than catalog hypocenter locations (Figure 11). Comparing our slip rate model to these hypocenters reveals a general correspondence between our modeled low slip rates and observed seismicity voids. However, this comparison comes with obvious caveats. The most distinct band of microseismicity traverses elements 42 and 45 (Figures 5c and 10), which our model estimates slip rate at 2.4 and 1.4 mm/yr, respectively. If the area of the microseismicity (about one third of the total element) is accounting for all the slip, we can apply a simple area ratio and estimate that the microseismicity streak is moving at ~6 mm/yr. Other areas that are devoid of microseismicity include portions of elements 32, 33, 35, 36, 39, 41, and 44 (all with slip rates less than 6 mm/yr). The distinct bands of seismicity suggest slip is occurring on the fault element. However, regions surrounding these bands are areas that are devoid of microseismicity. An exact correspondence between the microseismicity and model elements is not possible due to the limited spatial resolution of our model. However, the regions of slip deficit generally correspond to

Figure 10. (opposite) Model resolution shown by (a) value of the resolution matrix diagonal for the Calaveras fault segments and (b) the entire resolution matrix. Resolution values approach 1 for well-resolved elements. In Figure 10a, note the relatively strong resolution for the shallow and middle depth fault elements (0–6 km). The model resolution was calculated by fixing unit slip on each element and performing forward modeling to obtain the surface displacement field. The predicted surface displacement field was then back substituted into the inverse model and the estimated fault slip distribution was recovered. Predicted surface displacements were given data uncertainties used in the original fault slip modeling prior to back substitution. In Figure 10b, note the strong concentration of nonzero values of the resolving kernel about the diagonal elements. Also note the off-diagonal spread involving nearby faults due to the model smoothing. Arrows point to an example of the slip rate spread for element 111, the shallow creeping segment of the San Andreas fault south of Hollister.

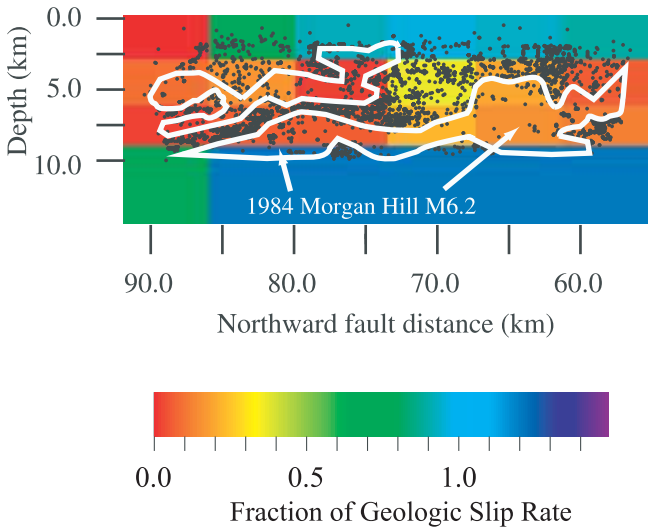

Figure 11. Comparison of fraction of geologic slip rates with precise relocations of seismicity from *Schaff et al.* [2002] along the Morgan Hill segment. Regions outlined in white exhibit sparse seismicity. Arrows point to the two areas of the Calaveras fault that had the greatest estimated slip during the 1984 M_L 6.2 Morgan Hill earthquake. The size of the discretized slip elements is too large to provide the detail revealed in the seismicity relocations; however, there is a general correspondence between low slip rates and low seismicity levels.

areas that have microseismicity voids, suggesting that there are locked areas within this region, which may be accumulated a slip deficit to be released in future events.

[40] Since the coseismic offsets and immediate postseismic effects have been removed from the geodetic data, we can readily observe that the region of interseismic slip deficit at the northern end of the Morgan Hill segment corresponds to the location of the 1984 M_L 6.2 Morgan Hill earthquake. On the basis of an average 11 mm/yr slip deficit for the area covered by elements 35, 36, 39, 42 and 44 over a period of 73 years (the period between the 1911 and 1984 events that occurred in this region [*Oppenheimer et al.*, 1990]), we calculate a M_w 6.2 event, which is similar to the 1984 event (Table 3). Additionally, if we consider region III identified by *Oppenheimer et al.* [1990] using typical recurrence intervals, we obtain events of similar magnitude.

[41] Seismicity for the Alum Rock segment is limited to the southern region and is typically at depths of 6–9 km. Our modeled slip rates in the seismogenic zone for this segment are at or near zero. *Oppenheimer et al.* [1990] suggested three small locked areas for the Alum Rock segment (regions IV, V, and VI). We combine all three of these regions in Figure 5c since the size of our model elements limits our ability to address these regions separately. Region IV had events in 1943 and 1988, both with M_L 5.1 [*Oppenheimer et al.*, 1990]. An estimated slip deficit of 5 mm/yr for model element 49 corresponding to this region over the 45-year intervening period, produces an estimated M_w 5.4 event (Table 3). A similar result is achieved when looking at the 1955 M_L 5.5 and 1996 M_w 4.7 events in region V. The estimated magnitudes based on our model results are likely high, since the areas of slip of suspected locked regions are smaller than the size of the model elements. However, the magnitudes are generally consistent with the size of events in regions IV, V and VI.

[42] *Oppenheimer and Lindh* [1992] suggested that the entire northern Calaveras fault (the combined Sunol and San Ramon segments) is locked based on the absence of microseismicity. Most of the seismicity along the northern Calaveras fault is diffuse and scattered, with the most prominent clusters at the northern end of the Calaveras fault. These clusters are roughly SW-NE trending and are located to the northeast of the northern terminus of the Calaveras fault. The results of our model are in agreement with *Oppenheimer and Lindh* [1992] and suggest that the greater portion of the northern Calaveras fault is locked. The model slip values in the seismogenic zone are consistently zero for these segments, except for elements 67–68 which has a slip rate that is about one third of the long-term estimated deep slip rate. The only significant event on the northern Calaveras fault during historical time is the 1861 M_L 6.4 earthquake, which reportedly caused surface rupture on the Calaveras fault in the San Ramon Valley [*Simpson et al.*, 1992]. Using the 6 mm/yr slip deficit for the entire northern Calaveras fault and the 550 year recurrence interval from *Kelson et al.* [1996], we calculate a M_w 6.9 event. Using a 150 year recurrence interval, a M_w 6.5 event would result, which is similar in magnitude to the 1861 event presuming the entire northern segment was involved (Table 3).

[43] Although *Oppenheimer et al.* [1990] did not specifically address seismic gaps on the Hollister segment, an inspection of the microseismicity reveals a gap that may represent a locked region (Figure 5c). Model elements 15 and 16 loosely correspond to this seismic gap. Unfortunately, the seismic gap straddles the model elements and an exact correspondence is lacking. Given a slip rate deficit of 10 mm/yr for segments 15 and 16 accumulating over a period of 50 years, we calculate a hypothetical M_w 5.8 event. However, the historical behavior of this fault suggests that the segment is an unlikely source for moderate to large events. The closest notable event to this region is a M_L 4.5 that occurred in 1974 on the northeast striking Busch fault [*Oppenheimer et al.*, 1990]. Also, the rate of seismicity on the Hollister segment is low compared to the Coyote and Morgan Hill segments. Whether the absence of seismicity is suggestive of locked regions or simply aseismic creep is unknown. Although the fault creeps at rates approaching the long-term slip rate (suggestive of rigid block motion) [*Savage et al.*, 1979], the existence of small asperities cannot be discounted.

7. Conclusions

[44] The effective minimization of risks associated with earthquakes is dependent on an accurate characterization of seismic hazard. Understanding the behavior of all the major faults in the SFBR and the potential for these faults to produce damaging earthquakes is critical to protect life and property and to ensure the economic stability of the region. The Calaveras fault is a probable source for damaging earthquakes [*WG99*, 1999]. Detailed studies of seismicity following the 1988 Alum Rock earthquake by *Oppenheimer*

et al. [1990] and *Oppenheimer and Lindh* [1992] identified seven locked fault regions on the Calaveras fault. Our fault slip rate distribution model is derived from geodetic measurements of surface deformation, and provides an independent characterization of the fault behavior that can be used to verify the regions identified by seismicity patterns.

[45] Our fault slip model consistently identifies zones of slip rate deficit that generally correspond to the regions of sparse microseismicity and the locked regions suggested by *Oppenheimer et al.* [1990] and *Oppenheimer and Lindh* [1992]. The moment calculations derived from the estimated slip deficit and recurrence intervals are consistent with observed historical seismicity along the Calaveras fault. Our moment calculations based on estimated slip rate deficits suggest that these events have the potential to be of M_w 6–7. Events of this magnitude will likely cause significant damage to parts of the SFBR.

[46] In general, distributed fault slip rate modeling using geodetic data collected during interseismic periods can successfully be used in combination with seismicity patterns to identify specific fault regions that may be locked and accumulating strain. The identification of these locked regions ultimately permits better characterization of seismic hazards. The resolution of the inferred slip pattern ultimately depends on the precision and spatial density of the deformation measurements. In the future, continued geodetic monitoring, refinement of fault slip rate distribution models and more detailed comparisons with earthquake relocations and repeating sequences of microearthquakes similar to studies of the Hayward fault [*Bürgmann et al.*, 2000] may provide additional information to better characterize the seismic hazard due to the Calaveras fault.

[47] **Acknowledgments.** We thank Wayne Thatcher, Bob Simpson, D. J. Andrews, Jeff Freymueller, James Savage, and Mike Lisowski for their reviews, insightful comments and constructive criticism. This work was funded in part by grants from the U.S. Geological Survey National Earthquake Hazards Reduction Program (Grant 99HQGR0066), the Geological Society of America, the Cordell Durrell Fund and the University of California, Davis Graduate Student Fellowship fund and the Berkeley Seismological Laboratory contribution 02–10. We would like to thank those who helped collect GPS data, in particular Gary Hamilton, Jerry Svarc, Michael Poland, Jeff Light, Eric Cannon, Ed Mueller, and John Gurley. We also thank the San Francisco Water District, Santa Clara County Department of Parks and Recreation, the East Bay Municipal Utilities District, the East Bay Regional Parks District and many private landowners for permission to collect data on their property.

References

Andrews, D. J., D. H. Oppenheimer, and J. J. Lienkaemper, The Mission link between the Hayward and Calaveras faults, *J. Geophys. Res.*, *98*(B7), 12,083–12,095, 1993.

Aydin, A., and B. Page, Diverse Pliocene-Quaternary tectonics in a transform environment, San Francisco Bay region, California, *Geol. Soc. Am. Bull.*, *95*, 1303–1317, 1984.

Bürgmann, R., R. Arrowsmith, and T. Dumitru, Rise and fall of the southern Santa Cruz Mountains, California, from fission tracks, geomorphology, and geodesy, *J. Geophys. Res.*, *99*(B10), 20,181–20,202, 1994.

Bürgmann, R., P. Segall, M. Lisowski, and J. Svarc, Postseismic strain following the 1989 Loma Prieta earthquake from GPS and leveling measurements, *J. Geophys. Res.*, *102*(B3), 4933–4955, 1997.

Bürgmann, R., D. Schmidt, R. M. Nadeau, M. d'Alessio, E. Fielding, D. Manaker, T. V. McEvilly, and M. H. Murray, Earthquake potential along the Northern Hayward fault, California, *Science*, *289*, 1178–1182, 2000.

Du, Y., and A. Aydin, Stress transfer during three sequential moderate earthquakes along the central Calaveras fault, *California, J. Geophys. Res.*, *98*(B6), 9947–9962, 1993.

Du, Y., A. Aydin, and P. Segall, Comparison of various inversion techniques as applied to the determination of a geophysical deformation model for the 983 Borah Peak earthquake, *Bull. Seismol. Soc. Am.*, *82*(4), 1840–1866, 1992.

Erickson, L. L., User's manual for DIS3D: A three dimensional dislocation program with applications to faulting in the earth, M.S. thesis, Stanford Univ., Stanford, Calif., 1987.

Freymueller, J. T., M. H. Murray, and D. Castillo, Kinematics of the Pacific-North America plate boundary zone, northern California, *J. Geophys. Res.*, *104*(B4), 7419–7441, 1999.

Galehouse, J. S., Creep rates and creep characteristics of eastern San Francisco Bay area faults: 1979–1992, in *Proceedings of the Second Conference on Earthquake Hazards in the Eastern San Francisco Bay Area*, *Spec. Publ. Calif. Div. Mines Geol.*, *113*, 289–297, 1992.

Harris, R., and P. Segall, Detection of a locked zone at depth on the Parkfield, California segment of the San Andreas fault, *J. Geophys. Res.*, *92*(B6), 7945–7962, 1987.

Jennings, C. W., Fault activity map of California and adjacent areas, *Geol. Data Map 6*, 1 sheet, scale 1:750,000, with explanatory text (92 pp.), 1 plate, Calif. Div. of Mines and Geol., Sacramento, 1994.

Kelson, K. I., W. R. Lettis, and M. Lisowski, Distribution of geologic slip and creep along faults in the San Francisco Bay region, in *Proceedings of the Second Conference on Earthquake Hazards in the Eastern San Francisco Bay Area*, *Spec. Publ. Calif. Div. Mines Geol.*, *113*, 31–38, 1992.

Kelson, K. I., G. D. Simpson, W. R. Lettis, and C. C. Haraden, Holocene slip rate and earthquake recurrence of the northern Calaveras fault at Leyden Creek, California, *J. Geophys. Res.*, *101*(B3), 5691–5975, 1996.

Kelson, K. I., J. N. Baldwin, and C. E. Randolph, Late Holocene slip rate and amounts of coseismic rupture along the central Calaveras fault, San Francisco Bay area, California, Final Technical Report submitted to the National Earthquake Hazard Reduction Program, 26 pp., William Lettis & Associates, Inc., Walnut Creek, Calif., 1998.

Langbein, J., and H. Johnson, Correlated errors in geodetic time series: Implications for time-dependent deformation, *J. Geophys. Res.*, *102*(B1), 591–603, 1997.

Lisowski, M., J. C. Savage, and W. H. Prescott, The velocity field along the San Andreas fault in Central and Southern California, *J. Geophys. Res.*, *96*(B5), 8369–8389, 1991.

Marshall, G. A., R. S. Stein, and W. Thatcher, Faulting geometry and slip from co-seismic elevation changes: The October 17, 1989 Loma Prieta, California, earthquake, *Bull. Seismol. Soc. Am.*, *81*, 1660–1693, 1991.

Matsu'ura, M., D. D. Jackson, and A. Cheng, Dislocation model for aseismic crustal deformation at Hollister, California, *J. Geophys. Res.*, *91*(B12), 12,661–12,674, 1986.

McLaughlin, R. J., Stop 4, Sargent fault zone at Loma Prieta, in *Field Guide to Neotectonics of the San Andreas Fault System, Santa Cruz Mountains, in Light of the Loma Prieta Earthquake*, edited by D. P. Schwartz and D. J. Ponti, *U. S. Geol. Surv. Open File Rep., 90-0274*, 19–22, 1990.

Menke, W., *Geophysical data analysis: Discrete Inverse Theory, Int. Geophys. Ser.*, vol. 45, Academic, San Diego, Calif., 1989.

Oppenheimer, D. H., and A. G. Lindh, The potential for earthquake rupture of the northern Calaveras fault, in *Proceedings of the Second Conference on Earthquake Hazards in the Eastern San Francisco Bay Area*, *Spec. Publ. Calif. Div. Mines Geol.*, *113*, 233–240, 1992.

Oppenheimer, D. H., W. H. Bakun, and A. G. Lindh, Slip partitioning of the Calaveras fault, California, and prospects for future earthquakes, *J. Geophys. Res.*, *95*(B6), 8483–8498, 1990.

Prescott, W. H., and M. Lisowski, Strain accumulation along the San Andreas fault system east of San Francisco Bay, California, *Tectonophysics*, *97*, 41–56, 1983.

Prescott, W. H., M. Lisowski, and J. C. Savage, Geodetic measurement of crustal deformation on the San Andreas, Hayward, and Calaveras faults near San Francisco, California, *J. Geophys. Res.*, *86*(B11), 10,853–10,869, 1981.

Prescott, W. H., N. E. King, and G. Guohua, Preseismic, coseismic, and postseismic deformation associated with the 1984 Morgan Hill, California, earthquake, in *The 1984 Morgan Hill, California, Earthquake*, *Spec. Publ. Calif. Div. Mines Geol.*, *68*, 137–148, 1984.

Prescott, W. H., J. C. Savage, J. L. Svarc, and D. Manaker, Deformation across the Pacific-North America plate boundary near San Francisco, California, *J. Geophys. Res.*, *106*(B4), 6673–6682, 2001.

Rodgers, J. D., and J. M. Halliday, Exploring the Calaveras-Las Trampas fault junction in the Danville-San Ramon area, in *Proceedings of the Second Conference on Earthquake Hazards in the Eastern San Francisco Bay Area*, *Spec. Publ. Calif. Div. Mines Geol.*, *113*, 261–270, 1992.

Savage, J. C., and W. H. Prescott, Precision of Geodolite distance measurements for determining fault movements, *J. Geophys. Res.*, *78*, 6001–6008, 1973.

Savage, J. C., and W. H. Prescott, Asthenosphere readjustment and the earthquake cycle, *J. Geophys. Res.*, *83*(B7), 3369–3376, 1978.

Savage, J. C., W. H. Prescott, M. Lisowski, and N. King, Geodolite measurements of deformation near Hollister, California, 1971–1978, *J. Geophys. Res.*, *84*(B13), 7599–7615, 1979.

Schaff, D. P., G. H. R. Bokelmann, G. C. Beroza, F. Waldhauser, and W. L. Ellsworth, High-resolution image of Calaveras Fault seismicity, *J. Geophys. Res.*, *107*(B9), 2186, doi:10.1029/2001JB000633, 2002.

Segall, P., and M. V. Mathews, Displacement calculations from geodetic data and the testing of geophysical deformation models, *J. Geophys. Res.*, *93*(B12), 14,954–14,966, 1988.

Segall, P., R. Bürgmann, and M. Matthews, Loma Prieta earthquake, *J. Geophys. Res.*, *105*(B3), 5615–5634, 2000.

Simpson, G. D., W. R. Lettis, and K. I. Kelson, Segmentation model for the Northern Calaveras fault, Calaveras Reservoir to Walnut Creek, in *Proceedings of the Second Conference on Earthquake Hazards in the Eastern San Francisco Bay Area*, *Spec. Publ. Calif. Div. Mines Geol.*, *113*, 253–259, 1992.

Smith, G. A., The Ygnacio segment and the southern terminus of the Concord fault, in *Proceedings of the Second Conference on Earthquake Hazards in the Eastern San Francisco Bay Area*, *Spec. Publ. Calif. Div. Mines Geol.*, *113*, 241–247, 1992.

Steketee, J. A., Some geophysical applications of the elasticity theory of dislocations, *Can. J. Phys.*, *36*, 1168–1199, 1958.

Unruh, J. R., and W. R. Lettis, Kinematics of transpressional deformation in the eastern San Francisco Bay region, California, *Geology*, *26*(1), 19–22, 1998.

Working Group on California Earthquake Probabilities (WG99), Earthquake probabilities in the San Francisco Bay region: 2000 to 2030—A summary of findings, *U.S. Geol. Surv. Open File Rep.*, *99–517*, 36 pp., 9 figures, 8 tables, 1999.

Working Group on Northern California Earthquake Potential (WGNCEP), Database of potential sources for earthquakes larger than magnitude 6 in northern California, *U.S. Geol. Surv. Open File Rep., 96–705*, 39 pp., 4 tables, 13 figs., appendix, 1996.

R. Bürgmann, Berkeley Seismological Laboratory, Department of Earth and Planetary Science, University of California, 215 McCone Hall 4760, Berkeley, CA 94720–4760, USA. (burgmann@seismo.berkeley.edu)

J. Langbein, U.S. Geological Survey, 345 Middlefield Road, MS 977, Menlo Park, CA 94025, USA. (langbein@usgs.gov)

D. M. Manaker, Department of Geology, University of California, Davis, 1 Shields Avenue, Davis, CA 95616, USA. (manaker@geology.ucdavis.edu)

W. H. Prescott, UNAVCO, Inc., 3360 Mitchell Lane, Suite C, Boulder, CO 80301–2245, USA. (prescott@unavco.org)